

Deletion of intestinal epithelial AMP-activated protein kinase alters distal colon permeability but not glucose homeostasis

Séverine Olivier, Camille Pochard, Hanna Diounou, Vanessa Castillo, Jordane Divoux, Joshua Alcantara, Jocelyne Leclerc, Sandra Guilmeau, Camille Huet, Wafa Charifi, et al.

▶ **To cite this version:**

Séverine Olivier, Camille Pochard, Hanna Diounou, Vanessa Castillo, Jordane Divoux, et al.. Deletion of intestinal epithelial AMP-activated protein kinase alters distal colon permeability but not glucose homeostasis. Molecular metabolism, 2021, pp.101183. 10.1016/j.molmet.2021.101183 . inserm-03135283

HAL Id: inserm-03135283

https://inserm.hal.science/inserm-03135283

Submitted on 8 Feb 2021

HAL is a multi-disciplinary open access archive for the deposit and dissemination of scientific research documents, whether they are published or not. The documents may come from teaching and research institutions in France or abroad, or from public or private research centers.

L'archive ouverte pluridisciplinaire **HAL**, est destinée au dépôt et à la diffusion de documents scientifiques de niveau recherche, publiés ou non, émanant des établissements d'enseignement et de recherche français ou étrangers, des laboratoires publics ou privés.



Distributed under a Creative Commons Attribution - NonCommercial - NoDerivatives| 4.0 International License

Deletion of intestinal epithelial AMP-activated protein kinase alters distal colon permeability but not glucose homeostasis

Séverine Olivier[1#], Camille Pochard[2,3,4#], Hanna Diounou[1], Vanessa Castillo[5], Jordane Divoux[6], Joshua Alcantara[5], Jocelyne Leclerc[1], Sandra Guilmeau[1], Camille Huet[1], Wafa Charifi[1], Thibault V. Varin[7], Noëmie Daniel[7], Marc Foretz[1], Michel Neunlist[2,3,4], Benoit L. Salomon[6], Pradipta Ghosh[5,8], André Marette[7], Malvyne Rolli-Derkinderen[2,3,4*] and Benoit Viollet[1*]

Co-first authors
* Co-corresponding authors.

[1]Université de Paris, Institut Cochin, CNRS, INSERM, Paris, France
[2]UMR1235 TENS, Nantes, F-44093, France
[3]IMAD, Institut des Maladies de l'Appareil Digestif, Nantes, France
[4]Université de Nantes, Nantes, France
[5]Department of Cellular and Molecular Medicine, University of California San Diego, La Jolla, CA 92093, USA
[6]Sorbonne Université, INSERM, CNRS, Centre d'Immunologie et des Maladies Infectieuses (CIMI), Paris, France.
[7]Québec Heart and Lung Research Institute, Laval University, Québec, Québec, Canada
[8]Department of Medicine, University of California San Diego, La Jolla, CA 92093, USA

Corresponding authors: To whom correspondence should be addressed. Malvyne Rolli-Derkinderen, TENS - Faculté de Médecine, 1, Rue Gaston Veïl, 44035 NANTES cedex 1, France; E-mail: malvyne.derkinderen@univ-nantes.fr, Phone: +33-(0)240412974 and Benoit Viollet, Institut Cochin, 24 rue du faubourg Saint Jacques 75014 Paris, France; E-mail: benoit.viollet@inserm.fr, Phone: +33-(0)144412401.

Abstract

Objective: The intestinal epithelial barrier (IEB) restricts the passage from the lumen through the paracellular space of potentially harmful substances and microbes, and rupture of its integrity is associated with a variety of gastrointestinal disorders and extra-digestive diseases. Increased IEB permeability has been linked to disruption of metabolic homeostasis leading to obesity and type 2 diabetes. Interestingly, recent studies have uncovered compelling evidence that the AMP-activated protein kinase (AMPK) signaling pathway plays important role in the maintenance of epithelial cell barrier function. However, our understanding of the function of intestinal AMPK in the regulation of IEB and glucose homeostasis remains sparse.

Methods: We generated mice lacking the two α1 and α2 AMPK catalytic subunits specifically in intestinal epithelial cells (IEC AMPK KO) and determined the physiological consequences of intestinal-specific deletion of AMPK in response to high-fat diet (HFD)-induced obesity. We combined histological, functional and integrative analyses to interrogate the outcomes of gut AMPK loss on intestinal permeability *in vivo* and *ex vivo*, on the development of obesity and metabolic dysfunction. We also determined the impact of intestinal AMPK deletion in an inducible mouse model (i-IEC AMPK KO) by measuring IEB function, glucose homeostasis and composition of gut microbiota by fecal 16S rRNA sequencing.

Results: While there were no differences in *in vivo* intestinal permeability in WT and IEC AMPK KO mice, *ex vivo* transcellular and paracellular permeability, measured in Ussing chambers, were significantly increased in the distal colon of IEC AMPK KO mice. This was associated with a reduction in pSer425 GIV phosphorylation, a marker of leaky gut barrier. However, expression of tight junction proteins in intestinal epithelial cells and pro-inflammatory cytokines in the lamina propria were not different between genotypes. Although the HFD-fed AMPK KO mice displayed suppression of the stress polarity signaling pathway and a concomitant increase in colon permeability, loss of intestinal AMPK did not exacerbate body weight gain or adiposity. Deletion of AMPK was also not sufficient to alter glucose homeostasis or the glucose lowering action of metformin in control diet (CD)- or HFD-fed mice. Finally, CD-fed i-IEC AMPK KO mice also presented higher permeability in distal colon under homeostatic conditions but, surprisingly, this was not detected upon HFD feeding. Alteration in epithelial barrier function in i-IEC AMPK KO mice was associated with a shift in the gut microbiota composition with higher levels of *Clostridiales* and *Desulfovibrionales*.

Conclusion: Altogether our results have unraveled a significant role for intestinal AMPK in the maintenance of IEB integrity in distal colon but not in the regulation of glucose homeostasis. Our data also highlight the complex interaction between gut microbiota and host AMPK.

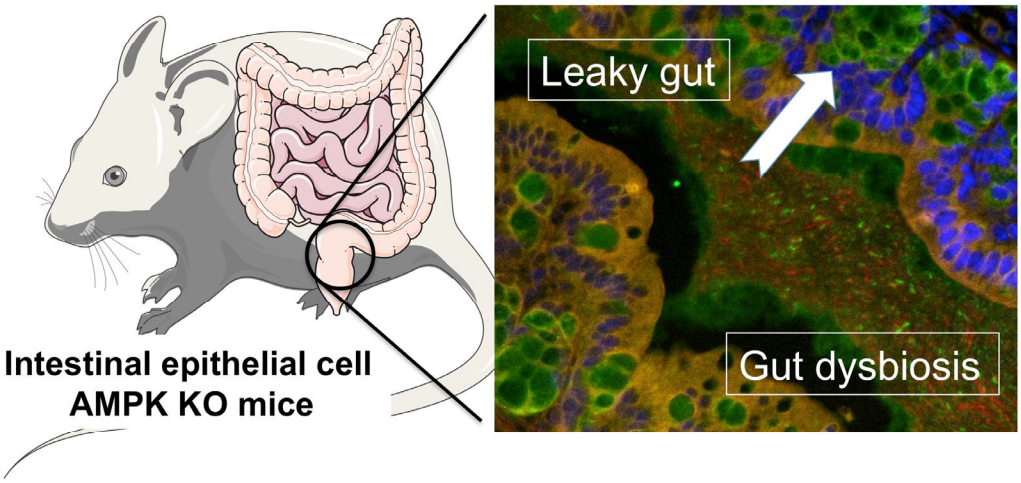
Keywords

AMPK, intestinal epithelial barrier (IEB), permeability, microbiota, obesity, metformin

Highlights

- Deletion of intestinal AMPKα1 and α2 suppresses the stress-polarity signaling (SPS) pathway.
- Loss of SPS-pathway is associated with increased paracellular permeability in distal colon.
- Intestinal AMPK is dispensable for the glucose lowering action of metformin.
- Loss of intestinal AMPK alters gut microbiota composition.

Graphical abstract



1. Introduction

The intestinal epithelial barrier (IEB) is a single-cell layer that constitutes the largest and the most important barrier to maintain an effective defense against intraluminal toxins, antigens, and enteric flora. Over the past decade, there has been increasing recognition of an association between disrupted IEB function and increased intestinal permeability or "leaky gut" in the pathogenesis and exacerbation of many chronic diseases. Altered intestinal permeability contributes to diseases primarily occurring within the gastrointestinal system, such as inflammatory bowel disease (IBD) and coeliac disease [1-3], and has been associated to clinical relapses in Crohn's disease [4]. Interestingly, the degree of intestinal permeability is also found to be associated with many of the risk factors for metabolic diseases [5; 6], suggesting that disrupted intestinal barrier could be an early event contributing to extra-digestive disease pathogenesis. The 'leaky gut' concept has been extended to the development of obesity and its metabolic complications associated with systemic low-grade inflammation [7]. It has been proposed that expansion of metabolic endotoxemia triggered by diet-induced obesity (DIO) in rodent models is a direct consequence of the alteration of the gut barrier function and the gut microbiota composition permitting the translocation of bacterial components such as lipopolysaccharides (LPS) into the systemic circulation and peripheral tissues [8-11]. Similar findings have been described in human obesity with increased circulating levels of LPS [12], a distinct gut microbiome signature [13] and impairment of intestinal barrier function [14] in various cohorts. Considering the contribution of increased intestinal permeability to digestive and systemic disease pathogenesis, alleviating gut leakiness appears to be an attractive therapeutic strategy.

AMPK is an evolutionarily-conserved fuel-sensitive protein kinase and a cellular nutrient sensor implicated in the regulation of energy homeostasis [15]. Once activated by energy balance deficit, AMPK initiates metabolic changes to reprogram metabolism by inhibiting non-essential anabolic ATP-consuming processes while stimulating ATP-delivering catabolic pathways [15]. Recent evidences have expanded the paradigm of AMPK as a metabolic sensor and to the more global concept that AMPK has broad effects on cellular function [16]. Pioneering studies in renal MDCK cells described the important role for AMPK in the maintenance of epithelial cell barrier functions and demonstrated that pharmacological activation of AMPK protected the structure and barrier function of tight junctions [17; 18]. The contribution of AMPK activation to intestinal barrier integrity has been recently illuminated in cultured intestinal epithelial cells under various stress conditions, including Ca^{2+} depletion-, ethanol-, LPS-, oxidative stress- or dextran sulfate sodium (DSS)-induced intestinal barrier injury [19-26]. It has been reported that AMPK phosphorylates tight junction proteins and the associated proteins cingulin and GIV/Girdin [27-30], providing a possible regulatory mechanism of AMPK on intestinal barrier function.

The gut microbiota is well known to influence host health and to play a key role in the development of obesity by acting through complex interactions [31-33]. Restoration of intestinal health by microbiome-related strategies to attenuate inflammation and

strengthen the epithelial barrier function has shown promising results both in obese patients and DIO rodent models [7; 34-38]. Interestingly, disruption of the gut microbiota has been associated with activation of AMPK in germ-free mice as reported in skeletal muscle and liver as well as in colonocytes to influence energy balance homeostasis [39; 40]. Furthermore, fermentation products, such as short-chain fatty acids (SCFAs), synthesized directly by the commensal bacteria, can exert some of their actions in skeletal muscle, liver and intestine through the activation of AMPK, thus contributing to improvement of whole body metabolism by affecting lipid oxidation, insulin sensitivity [41; 42] and intestinal barrier function [43-45]. Further studies have also involved AMPK in the therapeutic potential of various pharmacological and nutritional compounds against DSS-induced colitis [46-49]. However, AMPK activation has been paradoxically linked to intestinal barrier dysfunction in chronic intestinal inflammatory conditions by decreasing ZO-1 expression [50]. Thus, there is evidence to suggest that, depending on context, engaging AMPK activation may exert either a positive or negative influence on IEB integrity.

While there is promise in targeting the IEB through modulation of AMPK, a deeper understanding of its regulatory role on epithelial homeostasis must be reached. Here, to better understand the control exerted by AMPK on IEB function, we studied IEB permeability, junctional protein expression, gut inflammation susceptibility and gut microbiota composition in animals lacking the two AMPKα1 and AMPKα2 catalytic subunits in intestinal epithelial cells in response to high-fat diet (HFD)-induced obesity.

2. Material and Methods

2.1 Reagents and Antibodies

FITC- and TRITC-conjugated dextran (4 kDa) was obtained from TdB Consultancy AB. Horse radish peroxidase (HRP), red carmine and carboxymethylcellulose (CMC) were from Sigma. Primary antibodies directed against total AMPKα (#2532), AMPKβ1 (#4178), AMPKβ2 (#4148), AMPKγ2 (#2536), AMPKα phosphorylated at Thr-172 (#2531), total acetyl-CoA carboxylase 1/2 (ACC1/2) (#3676), ACC phosphorylated at Ser-79 (#3661) and β-actin (#4967) were purchased from Cell Signaling Technology. AMPKγ1 antibodies (#ab32508) were obtained from Abcam. ZO-1 antibodies were obtained from Cell Signaling Technology (#13663) and ThermoFisher Scientific (#33-9100, ThermoFisher Scientific). Anti-AMPKα1 and anti-AMPKα2 antibodies were kindly donated by Grahame Hardie (University of Dundee, Dundee, UK). HRP-conjugated secondary antibodies, goat anti-mouse IgG (#401215) and goat anti-rabbit IgG (#401393) were purchased from Calbiochem (EMD Millipore).

2.2 Experimental animals

All animal procedures were carried out in accordance with the EU guidelines for the protection of vertebra animals used for scientific purposes (2010/63/EU) and were approved by the Institutional Animal Care and Use Committee n°034 from Université de Paris (Protocol number CEEA34.BV.157.12 and APAFIS 14911-2017120813494332 v5). Mice were

maintained under controlled environment conditions (12-h light/dark cycle) with free access to water and standard mouse diet. Constitutive (IEC AMPK KO) and inducible (i-IEC AMPK KO) deletion of AMPKα1 and AMPKα2 in intestinal epithelial cells were obtained by crossing AMPK$\alpha1^{fl/fl}$/$\alpha2^{fl/fl}$ mice [51] and mice harboring the Cre recombinase or the tamoxifen-inducible Cre recombinase (CreERT2) under the control of the *villin* promoter, respectively [52]. All mice were kept on a C57/BL6J background. Routine genotyping was carried out by PCR on tail DNA using primer pairs for *AMPKα1* (forward: 5'-TAT TGC TGC CAT TAG GCT AC-3'; reverse: 5'-GAC CTG ACA GAA TAG GAT ATG CCC AAC CTC-3'; to yield amplification products of 586 bp for *AMPKα1*$^{+/+}$ allele and 682 bp for *AMPKα1*$^{fl/fl}$ allele; for *AMPKα2* (forward: 5'-GCT TAG CAC GTT ACC CTG GAT-3'; reverse: 5'-GTC TTC ACT GAA ATA CAT AGC A-3' to yield amplification products of 260 bp for A*MPKα2*$^{+/+}$ allele and 310 bp for *AMPKα2*$^{fl/fl}$ allele) and villin-Cre/ CreERT2 (forward: 5'- CAA GCC TGG CTC GAC GGC C-3' complementary to the villin promoter; reverse: 5'-CGC GAA CAT CTT CAG GTT CT-3' complementary to the Cre coding sequence, to yield an amplification product of 220 bp) [51-53]. To induce AMPK deletion in intestinal epithelial cells, i-IEC AMPK KO mice were treated either for 5 days by intraperitoneal (IP) injections of tamoxifen (1 mg/day) or by 5 days supplementation in the diet (400 mg/kg TAM citrate, AT155T70400, ssniff, Germany) for 5 days at weaning previous to the control diet (CD) and HFD challenge, followed one month later by 3 consecutive IP tamoxifen injections (1 mg/day). Littermates were used for all experiments.

2.3 Diet studies

Male mice were fed a CD (E15745-047, Ssniff, Germany) containing 70 kJ% carbohydrate, 10 kJ% fat, 20 kJ% protein or HFD (E15742-347, Ssniff, Germany) containing 21 kJ% carbohydrate, 60 kJ% fat (primarily lard), 19 kJ% protein. Starting at 10 weeks of age, co-housed WT and IEC AMPK KO mice received either CD or HFD for 10 weeks. At weaning, WT and i-IEC AMPK KO mice were stratified on the basis of their genotype and were assigned to separate cages to receive either CD or HFD for 16 weeks. To analyze whole-body composition, unanaesthetized mice were scanned using the NMR Minispec+ LF90II (Bruker Optics).

2.4 Measurement of intestinal permeability in vivo and ex vivo

For analysis of *in vivo* transcellular and paracellular intestinal permeability, mice were gavaged with a mix solution of 4 kDa TRITC-conjugated dextran (2 g/kg) and HRP (0.1 g/kg) in 0.5% carboxymethylcellulose. Whole gut transit time was determined by using 0.6 g/kg carmine red in the gavage solution and measuring the time of the appearance in the feces. For permeability measurement, mice were placed in individual cages and tail tip blood samples were collected at 4h after gavage. Plasma was analyzed for TRITC-dextran 4 kDa concentration with an automatic fluorescence microplate reader at 544 nm excitation and 580 nm emission wavelengths to determine paracellular permeability. In order to determine

transepithelial permeability, plasma HRP activity was measured by an enzyme activity assay with the reagent 3,3',5,5'-tetramethylbenzidine (TMB, BD Bioscience).

Ex vivo paracellular permeability of intestinal segments (jejunum, ileum, proximal colon, and distal colon) was determined by mounting the tissues in Ussing chambers (Physiological Instruments) as described previously [54]. Each chamber contains 2 mL of Ham (HAM/F12; Invitrogen) nutrient mixture maintained at 37 °C and continuously gasified with 95% O_2 and 5% CO_2. After 30 minutes of equilibration, 200 µL of apical medium are replaced by 200 µL of a mix solution containing 4 kDa FITC-conjugated dextran (20 mg/ml) and HRP (3.75 mg/ml). The fluorescence level of the basolateral aliquots (150 µL) was measured every 30 minutes over a period of 180 minutes using an automatic fluorescence microplate reader (Varioskan, Thermo Fisher Scientific) at 485 nm excitation and 520 nm emission wavelengths.

2.5 Tolerance tests

Plasma glucose was assessed at 0, 20, 40, 60, 80 and 100 min after oral glucose administration (2g/kg) in mice fasted for 6 h. Metformin tolerance was tested with a single oral administration of metformin (250 mg/kg) or vehicle (water) and after 30 minutes challenged with an oral glucose bolus of 1.5 g/kg of body weight. For insulin tolerance test, mice deprived of food for 4 h received an intraperitoneal injection of insulin (0.5 units/kg body weight; Actrapid, Novo Nordisk) and blood glucose levels were determined 0, 15, 30, 45, 60, and 90 min after injection. Blood glucose was measured in tail tip blood samples using a glucometer (Roche Diagnostics). The area under the curve was calculated using the trapezoidal rule.

2.6 In Vivo GLP-1 Secretion

Mice were fasted overnight and gavaged with 10 mg/kg sitagliptin (MSD) 45 min before gastric gavage with a bolus of 25% glucose in olive oil. Blood was sampled 15 min after glucose/ olive oil dosing gavage by retro-orbital venipuncture with heparin-coated capillaries in tubes containing 1% DPP IV inhibitor (Merck) and protease inhibitors (Sigma-Aldrich). Active GLP-1 plasma concentration was measured by ELISA (K150JVC-1, Meso Scale Diagnostics).

2.7 Plasma measurements

Blood was collected into heparin or EDTA-containing tubes, and centrifuged to separate plasma. Plasma lipid parameters were measured on an automated Monarch device (Instrumentation Laboratory Co). Plamsa lipid parameters were determined enzymatically with added enzymatic reagents (Diasys) for total cholesterol and triglyceride levels and an automated Monarch device (Instrumentation Laboratory Co) for non-esterified fatty acids (NEFA), glycerol, and β-hydroxybutyrate levels. Analysis of circulating cytokines (IL-6, TNF-α, and IFN-γ) was performed using a Meso Scale Discovery U-Plex kit for mouse cytokine profiling according to the manufacturer's instructions.

2.8 Indirect calorimetry

Indirect calorimetric measurements of whole energy expenditure, O_2 consumption, CO_2 production, respiratory exchange ratio (RER, calculated as volume of CO_2 produced to volume of O_2 consumed ratio), food intake, drink intake and locomotor activity (beam breaks) were performed using an indirect calorimeter system (TSE PhenoMaster/LabMaster System). Energy expenditure, CO_2 production and O_2 consumption were expressed by whole lean tissue mass extracted from the EchoMRIanalysis. Mice were adapted for 60 hours to the metabolic chamber, and parameters were measured during 5 consecutive days. Room temperature was kept constant (22°C ± 1°C). Mice were assessed under standard CD nutritional conditions and HFD challenge for 10 weeks.

2.9 Fecal sample collection, DNA extraction and 16s gene-based analysis

Fresh fecal samples were collected in sterile tubes, stored at -80°C and were processed for DNA extraction according to the ZymoBIOMICS DNA Microprep Kit (Zymo Research). Extracted DNA (100 ng) was processed for 16S rRNA amplification of the V3-V4 region and fecal microbiota profiling were acquired as previously described [55]. Sequence reads were analyzed using the dada2 package (v1.5.0; [56]) in R (http://www.R-project.org). Forward and reverse reads were first trimmed to remove low quality regions. Sequences with an expected error threshold > 2 and > 4 for the forward and reverse reads respectively, with ambiguous bases, and with quality score less than or equal to 2 were discarded. Denoised forward and reverse reads were merged and searched for chimeras. Taxonomic assignment of amplicon sequence variants (ASVs) was performed using the RDP classifier algorithm (v2,2; [57]) trained against the Silva database 132 [58]. To avoid biases generated in sequencing depth, the ASVs tables were rarified to an even depth of 19,991 sequences per sample. Potentially spurious ASVs with total abundance lower than 0.05% and that appeared less than three times in the entire dataset were removed.

2.10 Fecal lipocalin-2 quantification

Quantification of fecal lipocalin-2 (Lcn-2) levels was performed as previously described [59]. Briefly, frozen fecal samples were homogenized in sterile PBS at 100 mg/ml and then centrifuged at 12,000 rpm for 10 min at 4 °C. Lcn-2 levels were measured in the supernatants using Duoset murine Lcn-2 ELISA kit (R&D Systems).

2.11 Intestinal epithelial cell fractionation and lamina propria cell isolation

To isolate intestinal epithelial cells, either “whole” (scrapping the epithelial lining) or “villus enriched” cell isolation methods were used. Briefly, intestinal fragments were isolated, opened longitudinally and rinsed with PBS. The tissue were rotated for 30 minutes at 4°C in PBS containing 1.5 mM EDTA and protease inhibitors cocktail (Complete Protease Inhibitor Cocktail; Roche). Cells were recovered by centrifugation at 1500 rpm at 4°C for 5 minutes and cell pellets were snap frozen in liquid nitrogen, and stored at −80°C. For cell fractionation, the sequential isolation of intestinal epithelial cells along the crypt–villus axis

was performed as previously described [60; 61]. To isolate cells from the lamina propria, a Miltenyi Lamina Propria Dissociation Kit for mouse (Miltenyi) was used according to manufacturer's instruction.

2.12 Quantitative real-time PCR analysis

Fragments of the different intestinal segments were lysed in RA1 buffer (Machery-Nagel) and total RNA extraction was performed with the Nucleospin RNAII kit according to the manufacturer's recommendations (Machery-Nagel). One µg of purified mRNA was denatured and retro-transcribed using Superscript III reverse transcriptase (Invitrogen). PCR amplifications were performed using the Absolute Blue SYBR green fluorescein kit (Roche) and analyzed on the StepOnePlus system (Life Technologies). Relative gene expression was calculated using the comparative Ct ($2^{-\Delta\Delta Ct}$) method, where values were normalized to a housekeeping gene (ribosomal protein S6). The following primers (Sigma Aldrich) were used: Tumor necrosis factor alpha (TNFα; # NM_013693.3 Forward Primer : 5'-GAA CTT CGG GGT GAT CGG TCC-3', Reverse Primer : 5'-GCC ACT CCA GCT GCT CCT CC-3'), Interleukin 1 beta (IL-1β; # NM_008361.4, Forward Primer : 5'-GCC TCG TGC TGT CGG ACC CAT A-3', Reverse Primer : 5'-TTG AGG CCC AAG GCC ACA GGT-3'), Interleukin 6 (IL-6; # NM_031168.2, Forward Primer : 5'-TCC AGT TGC CTT CTT GGG AC-3', Reverse Primer : 5'-AGT CTC CTC TCC GGA CTT GT-3'), Zona occludens-1 (ZO-1; # NM_009386.2, Forward Primer : 5'-AAG AAT ATG GTC TTC GAT TGG-3', Reverse Primer : 5'-ATT TTC TGT CAC AGT ACC ATT TAT CTT C-3'), Occludin (# NM_008756.2, Forward Primer : 5'-GGT TAA AAA TGT GTC TGC AGG CAC-3', Reverse Primer : 5'-GAG GCT GCC TGA AGT CAT CCA C-3'), Zona occludens-2 (ZO-2; # NM_001198985.1, Forward Primer : 5'-CTAGACCCCCAGAGCCCCAGAAA-3', Reverse Primer : 5'-TCGCAGGAGTCCACGCATACAAG-3'), -Claudin 1 (# NM_016674.4 Forward Primer : 5'-AATTTCAGGTCTGGCGACAT-3', Reverse Primer : 5'-GGCCAAATTCATACCTGGCA-3'), Claudin 2 (# NM_016675.4, Forward Primer : 5'-GAAAGGACGGCTCCGTTTTC-3', Reverse Primer : 5'-TCTTCGGAGCCTGTTTGCTT-3'), Claudin 3 (# NM_009902.4, Forward Primer : 5'-GCCCCAGGAGAGGAGCCGTTAA-3', Reverse Primer : 5'-GCCGATGAAGGCCGAAACGC-3') and Ribosomal protein S6 (RPS6; # NM_001010.2, Forward Primer : 5'-CCA AGC TTA TTC AGC GTC TTG TTA CTC C-3', Reverse Primer : 5'-CCC TCG AGT CCT TCA TTC TCT TGG C-3').

2.13 Western Blotting

Cells were lyzed in ice-cold lysis buffer (50 mM Tris, pH 7.4, 1% Triton X-100, 150 mM NaCl, 1 mM EDTA, 1 mM EGTA, 10% glycerol, 50 mM NaF, 5 mM sodium pyrophosphate, 1 mM Na_3VO_4, 25 mM sodium-β-glycerophosphate, 1 mM DTT, 0.5 mM PMSF and protease inhibitors cocktail (Complete Protease Inhibitor Cocktail; Roche) and were sonicated on ice for 15 s to shear DNA and reduce viscosity. Intestine samples isolated from duodenum, jejunum, ileum and colon were homogenized in ice-cold lysis buffer using a ball-bearing homogenizer (Retsch). The homogenate was centrifuged for 10 min at 10,000× g at 4 °C, and the supernatants were removed for determination of total protein content with a BCA protein assay kit (Thermo Fisher Scientific). Proteins (25 µg) were separated by SDS-PAGE in

precast 4-15% polyacrylamide gels (Biorad) and the resulting bands were transferred to nitrocellulose membranes. Equal loading was checked by membrane staining with Ponceau Red before blocking with Tris-buffered saline supplemented with 0.2% NP40 and 5% non-fat dry milk for 30 min at room temperature. Immunoblotting was performed following standard procedures. Total pan-AMPKα, AMPKα1, α2, β1, β2, γ1, γ2 and β-actin and phosphorylated AMPK and ACC were probed from separated membranes. The signals were detected with chemiluminescence reagents (EMD Millipore) by using ImageQuant LAS 4000 (GE Healthcare) or X-ray films. Band intensities were quantified by Image J densitometry analysis and ratio for AMPKα1/AMPKα2 were calculated.

2.14 Flow cytometry analysis

Immune phenotyping of adipose tissue and colon biopsies was performed as followed. Mice were anesthetized using xylazine/ketamine and perfused by intra-cardiac injection of cold PBS before harvesting tissues. Small pieces of colon, removed from Peyer patches and epithelium, and adipose tissue were digested in type IV collagenase (1 mg/ml) and DNase I (10 µg/ml) for 30 min at 37°C, followed by Percoll gradient (40–80%) separation. Single cells suspension was then stained with lived dead-e780 (Thermofisher) for 10 min in cold PBS followed by 20 min incubation in cold PBS 3% FBS with the following mAbs: anti-$CD45_{LCA}$ (30-F11, BD-Bioscience), anti-CD11b (M1/70, BD-Bioscience), anti-CD11c (HL3 BD-Bioscience), anti-IA/E (M5/114.15.2, BD-Bioscience), anti-Ly6C (AL-21, BD-Bioscience), anti-Ly6G (1A8, BD-Bioscience), anti-F4/80 (BM8, Thermofisher). Cells were acquired on a Fortessa X20 cytometers (BD-Bioscience) and analyzed using FlowJo software (BD-Bioscience). Myeloid cells populations were defined as followed: Monocyte (CD45+CD11b+Ly-6C+); Dendritic cells (CD45+CD11c+IA/E+); Macrophage (CD45+CD11b+F4/80+); Neutrophils (CD45+Ly-6C+Ly-6G+).

2.15 Immunohistochemistry (pSer425 GIV)

Formalin-fixed paraffin-embedded colon sections of 4 µm thickness were cut and placed on glass slides coated with poly-L-lysine, followed by deparaffinization and hydration as previously described [28]. Heat-induced epitope retrieval was performed using sodium citrate buffer (pH 6) in a pressure cooker. Tissue sections were incubated with 0.3% hydrogen peroxidase for 15 min to block endogenous peroxidase activity, followed by incubation with primary antibodies for 30 min in a humidified chamber at room temperature. Antibodies used for immunostaining were anti-pS245 GIV (1:50, antirabbit antibody). Immunostaining was visualized with a labeled streptavidin–biotin using 3,3'-diaminobenzidine as a chromogen and counterstained with hematoxylin. Immunohistochemistry (IHC) images were randomly sampled at different 150x100 pixel regions of interest (ROI). The ROIs were analyzed using IHC Profiler [https://doi.org/10.1371/journal.pone.0096801]. IHC Profiler uses a spectral deconvolution method of DAB/hematoxylin color spectra by using optimized optical density vectors of the color deconvolution plugin for proper separation of the DAB color spectra. The histogram of

the DAB intensity was divided into 4 zones: high positive (0 to 60), positive (61 to 120), low positive (121 to 180) and negative (181 to 235). High positive, positive, and low positive percentages were combined to compute the final percentage positive for each ROI. The range of values for the percent positive is compared among different experimental groups.

2.16 Transmission Electron Microscopy

Colon samples were fixed in 3% glutaraldehyde, 0.1 M sodium phosphate buffer (pH 7.4) for 24 h at 4 °C, postfixed with 1% osmium tetroxide, dehydrated with 100% ethanol, and embedded in epoxy resin. For ultrastructure analysis, ultrathin slices (70–100 nm thick) were cut from the resin blocks with a Reichert Ultracut S ultramicrotome (Reichert Technologies, Depew, NY, USA), stained with lead citrate and uranyl acetate, and examined in a transmission electron microscope (model 1011; JEOL, Tokyo, Japan) at the Cochin Institute electron microscopy facility.

2.17 Statistical analyses

The R Phyloseq package (v1.26.1) was used to perform all microbiota diversity analyses. Shannon index was calculated to assess alpha diversity. Differences in beta diversity were visualized using principal coordinate analysis (PCoA) based on unweighted UniFrac distance calculated from 16S rRNA gene sequencing data. Detection of differentially abundant taxa between groups was performed with the metagenomics biomarker discovery tool linear discriminant analysis effect size (LefSe) [62]. A logarithmic LDA score of >2.5 was used as threshold.

Data are presented as means ± SEM. Results were analyzed using Student's t test, 2- or 3-way ANOVA with or without repeated measurements as appropriate followed by a Bonferroni post hoc test using the GraphPad Prism software. Values of $p < 0.05$ were considered statistically significant.

3. Results

3.1 AMPK α1 and α2 catalytic subunits are expressed along the GI tract.

To study the physiological role of AMPK in mouse GI tract, we first examined the distribution of AMPK isoforms in intestinal epithelial cells (IECs) isolated from the proximal and distal segments of the duodenum, jejunum, ileum and colon. We found that the AMPKα1 and AMPKα2 catalytic subunits and the AMPKβ1, AMPKβ2, AMPKγ1 and AMPKγ2 regulatory subunits are expressed at various levels along the small and large intestine (**Figure 1A**). Interestingly, an increasing gradient of both AMPKα1 and AMPKα2 protein expression was observed along the GI antero-posterior axis from the duodenum to the colon (**Figure 1A**). We also analyzed the pattern of AMPKα1 and AMPKα2 expression in the duodenum crypt-villus axis, where spatial expression changes and sub-specialization heterogeneity is well documented [63]. While AMPKα1 expression levels were not reliably changed, AMPKα2 displayed a decreasing gradient of expression from the villus tips to the

crypt resulting in a two-fold AMPKα1-to-AMPKα2 expression ratio in the crypt compartment (Suppl Fig. 1A and 1B). Next, to determine whether in response to the downregulation of one of the AMPKα catalytic subunit up-regulation of the remaining subunit can occur in the intestine, as previously reported in skeletal muscle, kidney or intestinal epithelial Caco-2 cells [23; 53; 64], we examined the expression of AMPKα1 and AMPKα2 in IECs isolated from global AMPKα1 KO and global AMPKα2 KO mice. Absence of AMPKα1 isoform was associated with increased levels of the AMPKα2 isoform and vice versa, suggesting compensatory mechanism to maintain intestinal homeostasis (Suppl Fig. 1C). Thus, to generate mice lacking AMPK activity in intestinal epithelium (IEC AMPK KO mice), we invalidated the two catalytic subunits of AMPK by crossing AMPKα1$^{fl/fl}$/α2$^{fl/fl}$ mice [51] with mice expressing Cre-recombinase under the control of the villin promoter, which drives expression in the epithelium of the GI tract [52]. The development and survival of animals were not impacted. IEC AMPK KO mice were born in Mendelian ratios and appeared normal at birth indistinguishable from their control littermates. There was no detectable AMPKα1 and AMPKα2 expression in IECs isolated from the small and large intestine of IEC AMPK KO mice but not control mice (**Figure 1A**). AMPKα1 and AMPKα2 expression was not altered in the liver and skeletal muscle, confirming the deletion is specific to IECs (Suppl Fig. 1D). The deletion of AMPKα1 and AMPKα2 was associated with a substantial reduction in the expression of the regulatory subunits AMPKβ1 and AMPKγ1, whereas expression of AMPKβ2 and AMPKγ2 was poorly altered (**Figure 1A**). No changes in body weight, length of the intestine and colon, total transit time, and humidity of feces were observed in IEC AMPK KO mice compared to WT mice (**Figures 1B-F**). In addition, there was no difference in the contractile activity of the GI tract between IEC AMPK KO and WT mice (Suppl Fig 2A and 2B). Necropsy revealed normal structure of the GI tract with similar intestinal epithelial cell distribution and no sign of spontaneous colitis was observed between IEC AMPK KO and WT mice. Hematoxylin and eosin staining or electron microscopy analysis of transverse sections of the small and large intestine showed no obvious abnormalities (Suppl Fig. 3A and 3B).

3.2 Deletion of AMPKα1 and AMPKα2 in IECs alters permeability in distal colon

To determine the role of AMPK in intestinal homeostasis, we assessed intestinal barrier permeability by measuring *in vivo* transcellular (HRP flux) and paracellular (4 kDa dextran flux) permeability. No difference was observed between IEC AMPK KO and WT mice using *in vivo* permeability measurements (**Figures 2A and 2B**). As AMPK activation has been associated with enhanced epithelial barrier function in Caco-2 intestinal epithelial cells [23; 24], we next examined more precisely the impact of AMPK deletion on gut integrity by measuring *ex vivo* transcellular and paracellular permeability with different segments of the GI tract in Ussing chambers. Interestingly, IEC AMPK KO mice display higher permeability exclusively in distal colon, indicating disrupted epithelial barrier function (**Figures 2C and 2D**). However, the mRNA expression of tight junction proteins ZO-1, ZO-2, occludin, claudin 1, claudin 2 and claudin 3 did not significantly differ in entire biopsies from distal colon (**Figure 2E**) and other segments of the small and large intestine (Suppl Fig. 3C) of IEC AMPK

KO and WT mice. The protein content of ZO-1 and occludin was also unaltered in the different portions of the GI tract from IEC AMPK KO compared to WT mice (Suppl Fig. 3D). As inflammation and IEB permeabilty are linked, we next analyzed whether cytokine mRNA expression are altered in IEC AMPK KO mice (**Figure 2G** and Suppl Fig. 3E). While the expression of pro-inflammatory cytokines IL-6 and IL-1β was similar in the distal colon from both genotypes, TNF-α mRNA expression levels tended to be slightly increased in the absence of gut AMPK (**Figure 2F**).

Furthermore, the observed leakiness in the IEC AMPK KO distal colon was associated also with the loss of a recently described polarity signaling pathway that is orchestrated by AMPK at the tight junctions of the epithelial lining of the gut [28; 65]. When we assessed stress polarity signaling (SPS)-pathway using a previously validated anti-phosphoSer245 Girdin antibody [28; 66], we found that the pathway is active in the WT but not IEC AMPK KO mice, specifically in the distal colon (**Figure 2F-I**). These findings are consistent with the fact that this pathway is triggered by microbes/microbial products that are encountered in increasing manner in the distal colon. Taken together, these findings demonstrate that the distal colon in IEC AMPK KO mice are leakier, and that such leakiness may at least in part be a consequence of an impaired AMPK-dependent barrier-protective pathway.

3.3 Constitutive intestinal AMPK deletion combined with HFD challenge does not exacerbate intestinal hyperpermeability.

Obesity is associated with intestinal hyperpermeability and metabolic endotoxemia [10; 67; 68]. Therefore, we evaluated the effects of AMPK deletion on intestinal permeability in response to a HFD challenge for 10 weeks (**Figure 3A**). Neither transcellular nor paracellular permeability was changed after HFD challenge. There were no differences in the *in vivo* transcellular (HRP flux) and paracellular (4 kDa dextran flux) permeability between IEC AMPK KO and WT mice at the completion of HFD challenge (**Figures 3B** and Suppl Fig. 4A). Again, an increased permeability is observed in the distal colon of HFD-fed IEC AMPK KO compared to WT (**Figure 3C**). As previously observed for CD, permeability in jejunum, ileum or proximal colon is comparable between WT and KO animals on HFD (Suppl Fig. 4B and 4C). No differences were observed on the mRNA expression of the tight junction protein ZO-1 in the intestinal epithelial layer (IEL) fraction of distal colon from HFD-fed IEC AMPK KO and WT mice (**Figure 3D**). While mRNA expression of the pro-inflammatory cytokines TNF-α and IL-1β was unchanged in the lamina propria layer (LPL) of distal colon from HFD-fed IEC AMPK KO and WT mice, there was a significant increase in IL-6 mRNA levels induced by the gut AMPK disruption (**Figure 3E**), suggesting alteration in the control of intestinal inflammation in IEC AMPK KO mice fed a HFD. However, there was no difference in circulating IL-6, TNF-α, and IFN-γ levels between IEC AMPK KO and WT mice fed a CD or HFD (**Figure 3F**).

3.4 Constitutive intestinal AMPK deletion does not exacerbate obesity-induced metabolic dysfunctions.

Next, to address whether lack of intestinal AMPK may induce metabolic dysfunction and exacerbate diet-induced obesity, we monitored changes in body weight between IEC AMPK KO and WT mice challenged with a CD or HFD for 10 weeks (**Figure 3A**). During the last week of diet exposure, there was no difference in body mass or adiposity between IEC AMPK KO and WT mice fed a regular CD, and while the HFD increased both body mass and adiposity, IEC AMPK KO mice gained similar amount of body weight or fat mass as the WT mice (**Figures 4A and 4B**). Consistently, no difference was observed between genotypes for food and drink intake, and spontaneous locomotor activity when animals were fed either a regular CD or HFD (**Figures 4C-E** and Suppl. Fig. 5A-C). We next investigated energy metabolism and found that IEC AMPK KO mice have a similar average energy expenditure (EE) compared to WT mice fed a CD or HFD during both the light and dark phases (**Figure 4F**). No significant changes in VCO_2, VO_2 and RER (VCO_2-to-VO_2 ratio) were observed during the light and dark phases between WT and IEC AMPK KO mice fed a CD or HFD, indicating similar oxidation capacity between genotypes (**Figures 4G-I**). However, a small but not significant trend (p= 0.0608) for increased RER was observed in IEC AMPK KO mice when fed a control diet (**Figure 4I**). There was no difference in post prandial triglyceride clearance from the circulation during an oral fat tolerance test by oral gavage of olive oil, indicating unaltered lipid absorption and maintenance of systemic lipid homeostasis between WT and IEC AMPK KO mice (Suppl. Fig. 5D). Plasma lipid parameters were not consistently affected by genotype in mice fed a regular CD or a HFD (Suppl. Fig. 5E). Glucose tolerance and insulin sensitivity were also similar between IEC AMPK KO and WT mice fed a CD or a HFD (**Figures 5A and 5B**). In addition, plasma GLP-1 levels were comparable in IEC AMPK KO and WT mice at basal state or after an oral challenge with a bolus of glucose in olive oil to stimulate GLP-1 secretion (Suppl. Fig. 5F). Overall these data indicate that the lack of AMPK in IECs does not promote or exacerbate the dysregulation of glucose homeostasis.

3.5 Intestinal AMPK is dispensable for the glucose lowering action of metformin.

Recent studies have reported that the GI tract contributes to the overall glucose lowering effect of the antidiabetic drug metformin [69]. Since a glucoregulatory role for AMPK activation in the duodenal mucosal layer has been demonstrated in response to infusion of metformin into the gut [70], we evaluated the improvement of glucose tolerance after oral dosing with metformin. Treating WT mice fed a CD or HFD with a single dose of 250 mg/kg metformin was capable to consistently lower glucose excursions during oral glucose tolerance test but the removal of IEC AMPK was ineffective on the glucose-lowering ability of metformin, indicating that acute glycemic control by metformin is conferred independently of intestinal AMPK. (**Figures 5C and 5D**).

3.6 Inducible intestinal AMPK deletion does not impact on obesity-induced metabolic dysfunctions.

To investigate whether intestinal AMPK could shape the gut microbiota, we analyzed changes in microbiota composition in response to HFD in mice lacking IEC AMPK. To

circumvent potential effects of AMPK removal on microbiota composition prior to the HFD challenge, we generated an inducible deletion of both AMPKα1 and AMPKα2 in IECs by crossing AMPKα1$^{fl/fl}$/α2$^{fl/fl}$ mice with transgenic mice expressing a tamoxifen-dependent Cre recombinase (Cre-ERT2) under the control of the villin promoter [52]. After tamoxifen treatment, i-IEC AMPK KO mice displayed no detectable AMPKα1 and AMPKα2 expression in IECs isolated from small and large intestine segments (Suppl Fig. 6A). We next evaluated the effects of the inducible deletion of intestinal AMPK at weaning prior to a challenge with a CD or HFD for 16 weeks (**Figure 6A**). At the end of diet intervention, we checked that there were no more detectable AMPKα1 and AMPKα2 expression in IECs isolated from GI tract of i-IEC AMPK KO and WT mice (**Figure 6B**). Body weight gain and adiposity were similar in both genotypes fed either a regular CD or HFD (**Figures 6C and 6D** and Suppl Fig. 6B). These findings are consistent with the absence of difference in macrophage, neutrophil, dendritic cell and monocyte numbers in visceral adipose tissue of i-IEC AMPK KO and WT mice fed a CD or HFD (Suppl Fig. 6C). There was also no difference in overall glucose excursion during an oral glucose tolerance test between i-IEC AMPK KO and WT mice fed a CD or HFD (**Figure 6E**).

3.7 Inducible intestinal AMPK deletion modulates the composition of gut microbiota in CD- but not HFD-fed mice.

We collected stool samples from WT and i-IEC AMPK KO mice fed a CD or HFD for 16 weeks and fecal microbiota composition was analyzed by 16S rRNA gene-based sequencing. Principal coordinate analysis (PCoA) based on unweighted Unifrac-based distances showed a clear separation between gut communities of CD- and HFD-fed mice (**Figure 7A**). Likewise, the Shannon α-diversity of gut microbiota was slightly increased in HFD-fed mice (**Figure 7B**). Results from *t* tests showed that the average Shannon indices were significantly different between CD-fed WT mice and WT and i-IEC AMPK KO mice on HFD (p-value: 0.012 and 0.021, respectively) (**Figure 7B**). Interestingly, the gut microbiota composition was substantially altered in CD-fed i-IEC AMPK KO mice compared to CD-fed WT mice but the difference was lost when i-IEC AMPK KO and WT mice were fed a HFD (**Figure 7C**). In accordance with PCoA results, relative abundance of bacterial orders in each group highlighted the impact of HFD on gut microbiota and the differences between WT and i-IEC AMPK KO mice fed a CD. We found that the percentages of *Clostridiales* and *Desulfovibrionales* were seemed enriched in CD-fed i-IEC AMPK KO mice, whereas CD-fed WT mice showed increased proportions of *Erysipelotrichales* (**Figure 7C**). Challenge with HFD induced an increase in *Clostridiales* and *Lactobacillales* and a decrease in *Bacteroidales* and *Bifidobacteriales*. However, we did not observe major differences between microbiota of WT and i-IEC AMPK KO mice under HFD, except a decrease of *Verrucomicrobiales* in i-IEC AMPK KO mice (**Figure 7C**). Then, we analyzed the gut microbiota at a deeper taxonomic (genus-) level and identified individual taxa modulated selectively in the different groups of mice (**Figure 7D**). We next used linear discriminant analysis (LDA) effect size (LEfSe) to examine statistical differences in the relative abundance of gut microbiota between genotypes. By

selecting strong associations in the LDA (LDA scores >3), we showed that *Parasutterella* and *Parvibacter* were more abundant in WT mice under CD whereas *GCA-900066225*, *Dubosiella*, *Roseburia*, *Anaerovorax*, *Alloprevotella*, *Enterorhabdus, Desulfovibrionaceae* and genera from *Clostridiales* order and *Lachnospiraceae-NK4A136* group were more abundant in i-IEC AMPK KO mice (**Figure 7E**). Unlike CD-fed mice, bacterial composition was very similar between WT and i-IEC AMPK KO mice fed a HFD. We could however notice an increase of *Parvibacter* in WT mice and, interestingly, the abundance of *Akkermansia*, well known for improving gut barrier function [71], was decreased in i-IEC AMPK KO mice (**Figure 7F**).

3.8 Inducible deletion of intestinal AMPK does not worsen obesity-induced hyperpermeability.

We next aimed to determine if inducible deletion of intestinal AMPK influenced intestinal integrity in the same manner than following constitutive deletion. The *in vivo* paracellular permeability (4 kDa dextran flux) was similar between WT and i-IEC AMPK KO mice fed a regular CD or HFD (**Figure 8A**). In contrast, measure of *ex vivo* paracellular permeability revealed a dramatic increase in permeability in the distal colon from i-IEC AMPK KO mice fed a regular CD but not when challenged with a HFD (**Figure 8B**). Of note, intestinal permeability was not different in the jejunum from i-IEC AMPK KO and WT mice fed a CD or HFD (Suppl Fig. 6D). Expression levels of pro-inflammatory cytokines IL-6 and TNF-α were also similar in the distal colon from WT and i-IEC AMPK KO mice fed a CD or HFD but those of IL-1β were slightly decreased in i-IEC AMPK KO mice fed HFD (**Figure 8D**). Accordingly, fecal Lcn-2 levels, a sensitive and broadly dynamic marker of intestinal inflammation [59], were not different between genotypes on CD or HFD (**Figure 8E**). There were also no differences in the percentage of macrophage and monocyte among $CD45^+$cells in colon from i-IEC AMPK KO and WT mice fed a CD or HFD (Suppl Fig. 6E). Measure of circulating IL-6, TNF-α, and IFN-γ levels revealed no difference between genotypes on CD or HFD (**Figure 8F**). Expression levels of tight junction protein occludin was unchanged in the distal colon from WT and i-IEC AMPK KO mice fed a CD or HFD but those of ZO-1 were slightly decreased in i-IEC AMPK KO mice (**Figure 8G**). Taken together, these data indicate that while inducible AMPK deletion alters gut barrier integrity in distal colon in CD-fed i-IEC AMPK KO mice, HFD challenge seems to blur the impact of the lack of intestinal AMPK.

4. Discussion

While the GI tract is of growing therapeutic interest, little information exists on the expression and the distribution of AMPK in the small and large intestine. Previous studies have reported the predominance of AMPKα1 catalytic isoform expression in human colon carcinoma Caco2 cells [23; 72]. We show that both catalytic isoforms AMPKα1 and AMPKα2 are expressed along the mouse GI tract following an antero-posterior gradient. The observation that AMPKα2 overexpression compensated for loss of AMPKα1 in the GI tract of

AMPKα1 KO mice, and *vice versa*, led us to generate a mouse model without intestinal AMPK activity by deleting both AMPKα1 and AMPKα2 catalytic subunits. Although this mouse model does not permit to analyze the catalytic isoform-specific contributions, we cannot exclude that intestinal AMPKα1- and AMPKα2-containing heterotrimers have different phosphorylation targets and functions. Recent studies have reported that mice harboring an intestinal-specific ablation of AMPKα1 display impairment in intestinal barrier function, epithelial differentiation and long-chain fatty acids uptake [24; 73], indicating absence of AMPKα2 isoform signaling redundancy in this context. Furthermore, the antero-posterior graded distributions of the various catalytic and regulatory AMPK isoforms suggest diverse functional roles serving different physiological means to regulate GI homeostasis. Hence, further work is warranted to elucidate potential AMPK isoform-specific roles along the GI tract.

Using loss of function approaches, we report that AMPK is necessary for the control of paracellular permeability in distal colon, based on analysis in Ussing chambers. The correct establishment of cell-cell contact is crucial to maintain epithelial barrier function. The integrity of apical junctional organization, including tight junctions (TJs) and adherens junctions (AJs), plays a major role in the determination of mucosal permeability and its disturbance leads to leaky gut [74]. It was first demonstrated that AMPK contributes to the assembly of epithelial TJs in renal MDCK cells [17; 18]. These findings were extended in intestinal cell lines, where AMPK activation was shown to promote TJs assembly associated with enhanced ZO-1 and occludin redistribution and decreased paracellular permeability [22-24; 43; 75]. Multiple AMPK effectors known to participate in apical junction formation and assembly have been described. It was found that AMPK-modulated paracellular permeability is associated with increased protein content for claudin 1, claudin 4, occludin, and ZO-1 at TJs [19; 76; 77]. It has been also reported that AMPK directly phosphorylates claudin 4 leading to enhanced interaction with occludin [77]. However, we noticed no relevant modifications in TJ proteins expression and distribution at plasma membrane in distal colon lacking AMPK. It has been proposed that AMPK-induced TJ assembly is mainly regulated by effectors of AMPK that orchestrate the interaction between apical junctions and cytoskeleton. A role for AMPK in regulating the association of TJs with cytoskeletal microtubule network has been demonstrated with the direct phosphorylation of the scaffold protein cingulin on multiple residues [29; 30]. Other studies suggested that AMPK activation might facilitate TJ assembly by phosphorylating afadin and inducing its association with ZO-1 [78]. Furthermore, the phosphorylation of the multimodular polarity scaffold G-alpha interacting vesicle associated (GIV) protein or Girdin by AMPK at Ser245 also participates in the protection of epithelium integrity by stabilizing TJs [66]. Recently, we used a “gut-in-a dish” model system consisting of polarized enteroid-derived monolayers (EMDs) from mouse colon to confirm that Girdin Ser245 phosphorylation was abolished in AMPK-null compared to WT EMDs treated with the pharmacologic AMPK activators metformin and A-769662 [28]. Additionally, we demonstrated that AMPK-null EMDs display impaired barrier integrity with

reduced trans-epithelial electrical resistance (TEER) in association with loss of Girdin Ser245 phosphorylation [28]. In the present work, we showed that the SPS-pathway is suppressed, as determined by decreased Girdin Ser245 phosphorylation, in the distal but not proximal colon of IEC AMPK KO mice. Thus, these findings raise the possibility that Girdin may serve as one of the effectors of AMPK at the TJs.

Recent studies have suggested that intestinal hyperpermeability has a pivotal role in HFD-induced body weight gain and fat mass development [10]. However, although loss of IEC AMPK induces alteration in distal colon permeability, here we observed absolutely no difference in adiposity or energy expenditure after HFD challenge between genotypes. This was consistent with absence of higher systemic inflammation and similar increased macrophage infiltration into adipose tissue in HFD-fed mice lacking IEC AMPK. These data suggest that alterations in distal colon permeability caused by AMPK deletion are not sufficient to exacerbate HFD-induced obesity and metabolic endotoxemia.

It is now widely accepted that the GI tract plays a determinant role in the regulation of glucose homeostasis. The gut is an important endocrine organ that secretes from specialized enteroendocrine cells, distributed along the GI tract, an array of gastrointestinal hormones, which regulate gastric emptying, appetite and postprandial glucose metabolism. The beneficial effects of metabolic surgery, such as Roux-en-Y gastric bypass surgery (RYGB), to reduce hyperglycemia and enhance insulin secretion independently of weight loss have highlighted the potential of gut signals modulation in the amelioration of type 2 diabetes [79; 80]. While deletion of both AMPKα1 and α2 from intestinal enteroendocrine L-cells has been shown to restrict GLP-1 secretion and induce glucose intolerance [81], we report that absence of AMPKα1 and α2 in the intestinal mucosal layer has no effect on GLP-1 release and IEC AMPK KO mice display similar glucose tolerance compared to WT mice under CD or HFD feeding. The reasons for the apparent discrepancy is the use of a mouse genetic model with AMPK deletion in both intestinal enteroendocrine L-cells and pancreatic α-cells in earlier studies [81]. Inactivation of AMPK in pancreatic α-cells may lead to compensatory adaptation of enteroendocrine L-cell function as reported in the cross-talk between islet and intestine endocrine cells to preserve glucose homeostasis during the development of obesity [82].

Clinical evidence suggests that the anti-diabetic effects of metformin, a successful diabetes type 2 drug, likely originate from its actions in the gut, involving gastrointestinal hormone signaling, bile acids pool, gut microbiota and the gut-brain axis [69]. However, a major controversy concerns the metformin's mode of action encompassing both AMPK-dependent and -independent mechanisms. Using IEC AMPK KO mice under CD or HFD feeding, we questioned the contribution of intestinal AMPK to the pharmacological outcomes of metformin treatment. We show that intestinal AMPK is not necessary for the improvement of glucose tolerance by acute metformin administration. Although a duodenal

AMPK-dependent pathway has been involved in metformin glucose-lowering effect [70], the differences between the present and earlier studies may result from experimental settings (measure of glucose tolerance vs. glucose production). Alternatively, all the pleiotropic properties of metformin independent of AMPK signaling may mask the AMPK-dependent metformin action in the regulation of glucose homeostasis [83].

It has been previously reported that SCFAs produced by bacterial fermentation of non-digestible dietary fibers can activate AMPK and contribute to tight junctions assembly in Caco-2 cells [22; 43]. Recent studies further highlighted an interesting link between gut microbiota composition and AMPK activity [41; 84].In the present work, we studied the impact of IEC AMPK deletion on gut microbiota composition using an inducible model to avoid potential compensatory mechanisms caused by AMPK deletion during development. In i-IEC AMPK KO mice fed a CD, we found a shift in the community of intestinal microbes demonstrating the impact of host intestinal epithelial AMPK on the composition of gut microbiota. Supporting our observations, it was recently reported that high-fiber diet changes in the microbial diversity and composition (e.g., higher proportions of *Akkermansia* and *Bifidobacterium*) were lost when AMPK was inhibited via supplementation of the non-specific AMPK inhibitor, Compound C, in drinking water [85]. Of note, the higher abundance of the *Desulfovibrionaceae* family in i-IEC AMPK KO mice is correlated with altered barrier function in distal colon. In accordance with these findings, mice and human patients suffering from ulcerative colitis, a disease associated with altered intestinal permeability, showed a high proportion of *Desulfovibrionaceae* [86; 87]. It is speculated that intestinal sulfate-reducing bacteria from the *Desulfovibrionaceae* family reduced mucosal thickness and facilitate contact between bacterial antigens and the mucosal immune system [87]. Other specific species (e.g., *Clostridiales, Dubosiella*, *Roseburia*, *Alloprevotella, Enterorhabdus, and Anaerovorax*) discriminating the gut microbiota composition between WT and i-IEC AMPK KO mice were also identified but the association with the pathological host status remains to be further investigated. In contrast, under HFD feeding no much difference in the relative abundance of bacterial orders were observed between WT and i-IEC AMPK KO mice. Likewise, the long-term HFD intake induced the same shift of microbiota populations in both WT and i-IEC AMPK KO mice, indicating comparable obesity-related gut dysbiosis between genotypes. This may explain why the difference in paracellular permeability in distal colon observed in WT and i-IEC AMPK KO fed a CD is totally abolished when these mice are fed a HFD for 16 weeks. In addition, although we noticed lower abundance of *Akkermansia* [37; 71] in HFD-fed i-IEC AMPK KO mice, this was not accompanied by increased body weight gain or metabolic dysfunction. Thus, the influence of HFD on gut microbiota and metabolic dysfunctions appears to be dominant over the alteration of distal colon permeability resulting from the exclusive loss of intestinal AMPK.

5. Conclusions

Altogether, our data support a role of intestinal AMPK in the maintenance of gut homeostasis under homeostatic and pathological conditions. However, we have found that intestinal AMPK is not required for the regulation of glucose homeostasis or the metformin glucose-lowering effect. In particular, we found that intestinal AMPK participates in the control of intestinal integrity and permeability, specifically in distal colon by acting on the maintenance of barrier function. Our results suggest that blunted pSer245 GIV phosphorylation in the absence of AMPK may contribute to altered colon permeability. Our results also highlight the interaction between gut microbiota and host intestinal AMPK but fecal transfer experiments are warranted to confirm the relevance of the observed shift in bacterial species. In future studies it will be interesting to examine whether targeting AMPK signaling via pharmacological and nutritional approaches may lead to new therapeutic avenues for leaky gut syndrome.

References

[1] Chang, J., Leong, R.W., Wasinger, V.C., Ip, M., Yang, M., Phan, T.G., 2017. Impaired Intestinal Permeability Contributes to Ongoing Bowel Symptoms in Patients With Inflammatory Bowel Disease and Mucosal Healing. Gastroenterology 153(3):723-731 e721.

[2] Vivinus-Nebot, M., Frin-Mathy, G., Bzioueche, H., Dainese, R., Bernard, G., Anty, R., et al., 2014. Functional bowel symptoms in quiescent inflammatory bowel diseases: role of epithelial barrier disruption and low-grade inflammation. Gut 63(5):744-752.

[3] Odenwald, M.A., Turner, J.R., 2013. Intestinal permeability defects: is it time to treat? Clin Gastroenterol Hepatol 11(9):1075-1083.

[4] Wyatt, J., Vogelsang, H., Hubl, W., Waldhoer, T., Lochs, H., 1993. Intestinal permeability and the prediction of relapse in Crohn's disease. Lancet 341(8858):1437-1439.

[5] Leech, B., McIntyre, E., Steel, A., Sibbritt, D., 2019. Risk factors associated with intestinal permeability in an adult population: A systematic review. Int J Clin Pract 73(10):e13385.

[6] Ohlsson, B., Orho-Melander, M., Nilsson, P.M., 2017. Higher Levels of Serum Zonulin May Rather Be Associated with Increased Risk of Obesity and Hyperlipidemia, Than with Gastrointestinal Symptoms or Disease Manifestations. Int J Mol Sci 18(3).

[7] Araujo, J.R., Tomas, J., Brenner, C., Sansonetti, P.J., 2017. Impact of high-fat diet on the intestinal microbiota and small intestinal physiology before and after the onset of obesity. Biochimie 141:97-106.

[8] Cani, P.D., Amar, J., Iglesias, M.A., Poggi, M., Knauf, C., Bastelica, D., et al., 2007. Metabolic endotoxemia initiates obesity and insulin resistance. Diabetes 56(7):1761-1772.

[9] Cani, P.D., Possemiers, S., Van de Wiele, T., Guiot, Y., Everard, A., Rottier, O., et al., 2009. Changes in gut microbiota control inflammation in obese mice through a mechanism involving GLP-2-driven improvement of gut permeability. Gut 58(8):1091-1103.

[10] Cani, P.D., Bibiloni, R., Knauf, C., Waget, A., Neyrinck, A.M., Delzenne, N.M., et al., 2008. Changes in gut microbiota control metabolic endotoxemia-induced inflammation in high-fat diet-induced obesity and diabetes in mice. Diabetes 57(6):1470-1481.

[11] Tilg, H., Zmora, N., Adolph, T.E., Elinav, E., 2020. The intestinal microbiota fuelling metabolic inflammation. Nature reviews. Immunology 20(1):40-54.

[12] Lassenius, M.I., Pietiläinen, K.H., Kaartinen, K., Pussinen, P.J., Syrjänen, J., Forsblom, C., et al., 2011. Bacterial endotoxin activity in human serum is associated with dyslipidemia, insulin resistance, obesity, and chronic inflammation. Diabetes Care 34(8):1809-1815.

[13] Lynch, S.V., Pedersen, O., 2016. The Human Intestinal Microbiome in Health and Disease. N Engl J Med 375(24):2369-2379.

[14] Genser, L., Aguanno, D., Soula, H.A., Dong, L., Trystram, L., Assmann, K., et al., 2018. Increased jejunal permeability in human obesity is revealed by a lipid challenge and is linked to inflammation and type 2 diabetes. J Pathol 246(2):217-230.

[15] Hardie, D.G., 2014. AMP-activated protein kinase: maintaining energy homeostasis at the cellular and whole-body levels. Annu Rev Nutr 34:31-55.

[16] Hardie, D.G., Lin, S.C., 2017. AMP-activated protein kinase - not just an energy sensor. F1000Res 6:1724.

[17] Zhang, L., Li, J., Young, L.H., Caplan, M.J., 2006. AMP-activated protein kinase regulates the assembly of epithelial tight junctions. Proc Natl Acad Sci U S A 103(46):17272-17277.

[18] Zheng, B., Cantley, L.C., 2007. Regulation of epithelial tight junction assembly and disassembly by AMP-activated protein kinase. Proc Natl Acad Sci U S A 104(3):819-822.

[19] Wang, B., Wu, Z., Ji, Y., Sun, K., Dai, Z., Wu, G., 2016. L-Glutamine Enhances Tight Junction Integrity by Activating CaMK Kinase 2-AMP-Activated Protein Kinase Signaling in Intestinal Porcine Epithelial Cells. J Nutr 146(3):501-508.

[20] Cao, S., Wang, C., Yan, J., Li, X., Wen, J., Hu, C., 2020. Curcumin ameliorates oxidative stress-induced intestinal barrier injury and mitochondrial damage by promoting Parkin dependent mitophagy through AMPK-TFEB signal pathway. Free Radic Biol Med 147:8-22.
[21] Wu, W., Wang, S., Liu, Q., Shan, T., Wang, Y., 2018. Metformin Protects against LPS-Induced Intestinal Barrier Dysfunction by Activating AMPK Pathway. Mol Pharm 15(8):3272-3284.
[22] Elamin, E.E., Masclee, A.A., Dekker, J., Pieters, H.J., Jonkers, D.M., 2013. Short-chain fatty acids activate AMP-activated protein kinase and ameliorate ethanol-induced intestinal barrier dysfunction in Caco-2 cell monolayers. J Nutr 143(12):1872-1881.
[23] Olivier, S., Leclerc, J., Grenier, A., Foretz, M., Tamburini, J., Viollet, B., 2019. AMPK Activation Promotes Tight Junction Assembly in Intestinal Epithelial Caco-2 Cells. Int J Mol Sci 20(20).
[24] Sun, X., Yang, Q., Rogers, C.J., Du, M., Zhu, M.J., 2017. AMPK improves gut epithelial differentiation and barrier function via regulating Cdx2 expression. Cell Death Differ 24(5):819-831.
[25] Chang, K.W., Kuo, C.Y., 2015. 6-Gingerol modulates proinflammatory responses in dextran sodium sulfate (DSS)-treated Caco-2 cells and experimental colitis in mice through adenosine monophosphate-activated protein kinase (AMPK) activation. Food Funct 6(10):3334-3341.
[26] Wongkrasant, P., Pongkorpsakol, P., Ariyadamrongkwan, J., Meesomboon, R., Satitsri, S., Pichyangkura, R., et al., 2020. A prebiotic fructo-oligosaccharide promotes tight junction assembly in intestinal epithelial cells via an AMPK-dependent pathway. Biomed Pharmacother 129:110415.
[27] Zhu, M.J., Sun, X., Du, M., 2018. AMPK in regulation of apical junctions and barrier function of intestinal epithelium. Tissue Barriers 6(2):1-13.
[28] Ghosh, P., Swanson, L., Sayed, I.M., Mittal, Y., Lim, B.B., Ibeawuchi, S.R., et al., 2020. The stress polarity signaling (SPS) pathway serves as a marker and a target in the leaky gut barrier: implications in aging and cancer. Life Sci Alliance 3(3).
[29] Ducommun, S., Deak, M., Sumpton, D., Ford, R.J., Nunez Galindo, A., Kussmann, M., et al., 2015. Motif affinity and mass spectrometry proteomic approach for the discovery of cellular AMPK targets: identification of mitochondrial fission factor as a new AMPK substrate. Cell Signal 27(5):978-988.
[30] Yano, T., Matsui, T., Tamura, A., Uji, M., Tsukita, S., 2013. The association of microtubules with tight junctions is promoted by cingulin phosphorylation by AMPK. J Cell Biol 203(4):605-614.
[31] Postler, T.S., Ghosh, S., 2017. Understanding the Holobiont: How Microbial Metabolites Affect Human Health and Shape the Immune System. Cell Metab 26(1):110-130.
[32] Cani, P.D., 2019. Microbiota and metabolites in metabolic diseases. Nat Rev Endocrinol 15(2):69-70.
[33] Sonnenburg, J.L., Backhed, F., 2016. Diet-microbiota interactions as moderators of human metabolism. Nature 535(7610):56-64.
[34] Dosoky, N.S., May-Zhang, L.S., Davies, S.S., 2020. Engineering the gut microbiota to treat chronic diseases. Appl Microbiol Biotechnol 104(18):7657-7671.
[35] Hiippala, K., Jouhten, H., Ronkainen, A., Hartikainen, A., Kainulainen, V., Jalanka, J., et al., 2018. The Potential of Gut Commensals in Reinforcing Intestinal Barrier Function and Alleviating Inflammation. Nutrients 10(8).
[36] Hiel, S., Gianfrancesco, M.A., Rodriguez, J., Portheault, D., Leyrolle, Q., Bindels, L.B., et al., 2020. Link between gut microbiota and health outcomes in inulin -treated obese patients: Lessons from the Food4Gut multicenter randomized placebo-controlled trial. Clin Nutr.
[37] Depommier, C., Everard, A., Druart, C., Plovier, H., Van Hul, M., Vieira-Silva, S., et al., 2019. Supplementation with Akkermansia muciniphila in overweight and obese human volunteers: a proof-of-concept exploratory study. Nat Med 25(7):1096-1103.
[38] Krumbeck, J.A., Rasmussen, H.E., Hutkins, R.W., Clarke, J., Shawron, K., Keshavarzian, A., et al., 2018. Probiotic Bifidobacterium strains and galactooligosaccharides improve intestinal barrier function in obese adults but show no synergism when used together as synbiotics. Microbiome 6(1):121.

[39] Donohoe, D.R., Garge, N., Zhang, X., Sun, W., O'Connell, T.M., Bunger, M.K., et al., 2011. The microbiome and butyrate regulate energy metabolism and autophagy in the mammalian colon. Cell Metab 13(5):517-526.
[40] Backhed, F., Manchester, J.K., Semenkovich, C.F., Gordon, J.I., 2007. Mechanisms underlying the resistance to diet-induced obesity in germ-free mice. Proc Natl Acad Sci U S A 104(3):979-984.
[41] Araujo, J.R., Tazi, A., Burlen-Defranoux, O., Vichier-Guerre, S., Nigro, G., Licandro, H., et al., 2020. Fermentation Products of Commensal Bacteria Alter Enterocyte Lipid Metabolism. Cell Host Microbe 27(3):358-375 e357.
[42] Carvalho, B.M., Guadagnini, D., Tsukumo, D.M.L., Schenka, A.A., Latuf-Filho, P., Vassallo, J., et al., 2012. Modulation of gut microbiota by antibiotics improves insulin signalling in high-fat fed mice. Diabetologia 55(10):2823-2834.
[43] Peng, L., Li, Z.R., Green, R.S., Holzman, I.R., Lin, J., 2009. Butyrate enhances the intestinal barrier by facilitating tight junction assembly via activation of AMP-activated protein kinase in Caco-2 cell monolayers. J Nutr 139(9):1619-1625.
[44] Elamin, E., Jonkers, D., Juuti-Uusitalo, K., van Ijzendoorn, S., Troost, F., Duimel, H., et al., 2012. Effects of ethanol and acetaldehyde on tight junction integrity: in vitro study in a three dimensional intestinal epithelial cell culture model. PLoS One 7(4):e35008.
[45] Li, Q., Chen, H., Zhang, M., Wu, T., Liu, R., 2019. Altered short chain fatty acid profiles induced by dietary fiber intervention regulate AMPK levels and intestinal homeostasis. Food Funct 10(11):7174-7187.
[46] Bibi, S., Kang, Y., Du, M., Zhu, M.J., 2018. Dietary red raspberries attenuate dextran sulfate sodium-induced acute colitis. J Nutr Biochem 51:40-46.
[47] Gai, L., Chu, L., Xia, R., Chen, Q., Sun, X., 2019. Barbaloin Attenuates Mucosal Damage in Experimental Models of Rat Colitis by Regulating Inflammation and the AMPK Signaling Pathway. Med Sci Monit 25:10045-10056.
[48] Wei, W., Ding, M., Zhou, K., Xie, H., Zhang, M., Zhang, C., 2017. Protective effects of wedelolactone on dextran sodium sulfate induced murine colitis partly through inhibiting the NLRP3 inflammasome activation via AMPK signaling. Biomed Pharmacother 94:27-36.
[49] Zhou, K., Cheng, R., Liu, B., Wang, L., Xie, H., Zhang, C., 2018. Eupatilin ameliorates dextran sulphate sodium-induced colitis in mice partly through promoting AMPK activation. Phytomedicine 46:46-56.
[50] Scharl, M., Paul, G., Barrett, K.E., McCole, D.F., 2009. AMP-activated protein kinase mediates the interferon-gamma-induced decrease in intestinal epithelial barrier function. J Biol Chem 284(41):27952-27963.
[51] Boudaba, N., Marion, A., Huet, C., Pierre, R., Viollet, B., Foretz, M., 2018. AMPK Re-Activation Suppresses Hepatic Steatosis but its Downregulation Does Not Promote Fatty Liver Development. EBioMedicine 28:194-209.
[52] el Marjou, F., Janssen, K.P., Chang, B.H., Li, M., Hindie, V., Chan, L., et al., 2004. Tissue-specific and inducible Cre-mediated recombination in the gut epithelium. Genesis 39(3):186-193.
[53] Viollet, B., Andreelli, F., Jorgensen, S.B., Perrin, C., Geloen, A., Flamez, D., et al., 2003. The AMP-activated protein kinase alpha2 catalytic subunit controls whole-body insulin sensitivity. J Clin Invest 111(1):91-98.
[54] De Quelen, F., Chevalier, J., Rolli-Derkinderen, M., Mourot, J., Neunlist, M., Boudry, G., 2011. n-3 polyunsaturated fatty acids in the maternal diet modify the postnatal development of nervous regulation of intestinal permeability in piglets. J Physiol 589(17):4341-4352.
[55] Anhê, F.F., Nachbar, R.T., Varin, T.V., Trottier, J., Dudonné, S., Le Barz, M., et al., 2019. Treatment with camu camu (Myrciaria dubia) prevents obesity by altering the gut microbiota and increasing energy expenditure in diet-induced obese mice. Gut 68(3):453-464.
[56] Callahan, B.J., McMurdie, P.J., Rosen, M.J., Han, A.W., Johnson, A.J., Holmes, S.P., 2016. DADA2: High-resolution sample inference from Illumina amplicon data. Nat Methods 13(7):581-583.

[57] Wang, Q., Garrity, G.M., Tiedje, J.M., Cole, J.R., 2007. Naive Bayesian classifier for rapid assignment of rRNA sequences into the new bacterial taxonomy. Appl Environ Microbiol 73(16):5261-5267.
[58] Quast, C., Pruesse, E., Yilmaz, P., Gerken, J., Schweer, T., Yarza, P., et al., 2013. The SILVA ribosomal RNA gene database project: improved data processing and web-based tools. Nucleic Acids Res 41(Database issue):D590-596.
[59] Chassaing, B., Srinivasan, G., Delgado, M.A., Young, A.N., Gewirtz, A.T., Vijay-Kumar, M., 2012. Fecal lipocalin 2, a sensitive and broadly dynamic non-invasive biomarker for intestinal inflammation. PLoS One 7(9):e44328.
[60] Guilmeau, S., Flandez, M., Bancroft, L., Sellers, R.S., Tear, B., Stanley, P., et al., 2008. Intestinal deletion of Pofut1 in the mouse inactivates notch signaling and causes enterocolitis. Gastroenterology 135(3):849-860, 860 e841-846.
[61] Mariadason, J.M., Nicholas, C., L'Italien, K.E., Zhuang, M., Smartt, H.J., Heerdt, B.G., et al., 2005. Gene expression profiling of intestinal epithelial cell maturation along the crypt-villus axis. Gastroenterology 128(4):1081-1088.
[62] Segata, N., Izard, J., Waldron, L., Gevers, D., Miropolsky, L., Garrett, W.S., et al., 2011. Metagenomic biomarker discovery and explanation. Genome Biol 12(6):R60.
[63] Moor, A.E., Harnik, Y., Ben-Moshe, S., Massasa, E.E., Rozenberg, M., Eilam, R., et al., 2018. Spatial Reconstruction of Single Enterocytes Uncovers Broad Zonation along the Intestinal Villus Axis. Cell 175(4):1156-1167 e1115.
[64] Lieberthal, W., Tang, M., Zhang, L., Viollet, B., Patel, V., Levine, J.S., 2013. Susceptibility to ATP depletion of primary proximal tubular cell cultures derived from mice lacking either the alpha1 or the alpha2 isoform of the catalytic domain of AMPK. BMC nephrology 14:251.
[65] Ghosh, P., 2017. The stress polarity pathway: AMPK 'GIV'-es protection against metabolic insults. Aging (Albany NY) 9(2):303-314.
[66] Aznar, N., Patel, A., Rohena, C.C., Dunkel, Y., Joosen, L.P., Taupin, V., et al., 2016. AMP-activated protein kinase fortifies epithelial tight junctions during energetic stress via its effector GIV/Girdin. Elife 5.
[67] Johnson, A.M., Costanzo, A., Gareau, M.G., Armando, A.M., Quehenberger, O., Jameson, J.M., et al., 2015. High fat diet causes depletion of intestinal eosinophils associated with intestinal permeability. PLoS One 10(4):e0122195.
[68] Damms-Machado, A., Louis, S., Schnitzer, A., Volynets, V., Rings, A., Basrai, M., et al., 2017. Gut permeability is related to body weight, fatty liver disease, and insulin resistance in obese individuals undergoing weight reduction. Am J Clin Nutr 105(1):127-135.
[69] Foretz, M., Guigas, B., Viollet, B., 2019. Understanding the glucoregulatory mechanisms of metformin in type 2 diabetes mellitus. Nat Rev Endocrinol 15(10):569-589.
[70] Duca, F.A., Cote, C.D., Rasmussen, B.A., Zadeh-Tahmasebi, M., Rutter, G.A., Filippi, B.M., et al., 2015. Metformin activates a duodenal Ampk-dependent pathway to lower hepatic glucose production in rats. Nat Med 21(5):506-511.
[71] Everard, A., Belzer, C., Geurts, L., Ouwerkerk, J.P., Druart, C., Bindels, L.B., et al., 2013. Cross-talk between Akkermansia muciniphila and intestinal epithelium controls diet-induced obesity. Proc Natl Acad Sci U S A 110(22):9066-9071.
[72] Harmel, E., Grenier, E., Bendjoudi Ouadda, A., El Chebly, M., Ziv, E., Beaulieu, J.F., et al., 2014. AMPK in the small intestine in normal and pathophysiological conditions. Endocrinology 155(3):873-888.
[73] Wu, W., Wang, S., Liu, Q., Shan, T., Wang, X., Feng, J., et al., 2020. AMPK facilitates intestinal long-chain fatty acid uptake by manipulating CD36 expression and translocation. FASEB J 34(4):4852-4869.
[74] Turner, J.R., 2009. Intestinal mucosal barrier function in health and disease. Nature reviews. Immunology 9(11):799-809.

[75] Sun, X., Du, M., Navarre, D.A., Zhu, M.J., 2018. Purple Potato Extract Promotes Intestinal Epithelial Differentiation and Barrier Function by Activating AMP-Activated Protein Kinase. Molecular nutrition & food research 62(4).
[76] Park, H.Y., Kunitake, Y., Hirasaki, N., Tanaka, M., Matsui, T., 2015. Theaflavins enhance intestinal barrier of Caco-2 Cell monolayers through the expression of AMP-activated protein kinase-mediated Occludin, Claudin-1, and ZO-1. Biosci Biotechnol Biochem 79(1):130-137.
[77] Xiang, R.L., Mei, M., Cong, X., Li, J., Zhang, Y., Ding, C., et al., 2014. Claudin-4 is required for AMPK-modulated paracellular permeability in submandibular gland cells. Journal of molecular cell biology 6(6):486-497.
[78] Zhang, L., Jouret, F., Rinehart, J., Sfakianos, J., Mellman, I., Lifton, R.P., et al., 2011. AMP-activated protein kinase (AMPK) activation and glycogen synthase kinase-3β (GSK-3β) inhibition induce Ca2+-independent deposition of tight junction components at the plasma membrane. J Biol Chem 286(19):16879-16890.
[79] Evers, S.S., Sandoval, D.A., Seeley, R.J., 2017. The Physiology and Molecular Underpinnings of the Effects of Bariatric Surgery on Obesity and Diabetes. Annu Rev Physiol 79:313-334.
[80] Amouyal, C., Castel, J., Guay, C., Lacombe, A., Denom, J., Migrenne-Li, S., et al., 2020. A surrogate of Roux-en-Y gastric bypass (the enterogastro anastomosis surgery) regulates multiple beta-cell pathways during resolution of diabetes in ob/ob mice. EBioMedicine 58:102895.
[81] Sayers, S.R., Reimann, F., Gribble, F.M., Parker, H., Zac-Varghese, S., Bloom, S.R., et al., 2016. Proglucagon Promoter Cre-Mediated AMPK Deletion in Mice Increases Circulating GLP-1 Levels and Oral Glucose Tolerance. PLoS One 11(3):e0149549.
[82] Dusaulcy, R., Handgraaf, S., Skarupelova, S., Visentin, F., Vesin, C., Heddad-Masson, M., et al., 2016. Functional and Molecular Adaptations of Enteroendocrine L-Cells in Male Obese Mice Are Associated With Preservation of Pancreatic α-Cell Function and Prevention of Hyperglycemia. Endocrinology 157(10):3832-3843.
[83] Waise, T.M.Z., Rasti, M., Duca, F.A., Zhang, S.Y., Bauer, P.V., Rhodes, C.J., et al., 2019. Inhibition of upper small intestinal mTOR lowers plasma glucose levels by inhibiting glucose production. Nature communications 10(1):714.
[84] Koh, A., Mannerås-Holm, L., Yunn, N.O., Nilsson, P.M., Ryu, S.H., Molinaro, A., et al., 2020. Microbial Imidazole Propionate Affects Responses to Metformin through p38γ-Dependent Inhibitory AMPK Phosphorylation. Cell Metab.
[85] Li, Q., Zhang, M., Wu, T., Liu, R., 2020. Potential correlation between carbohydrate-active enzyme family 48 expressed by gut microbiota and the expression of intestinal epithelial AMP-activated protein kinase β. J Food Biochem 44(2):e13123.
[86] Håkansson, Å., Tormo-Badia, N., Baridi, A., Xu, J., Molin, G., Hagslätt, M.L., et al., 2015. Immunological alteration and changes of gut microbiota after dextran sulfate sodium (DSS) administration in mice. Clin Exp Med 15(1):107-120.
[87] Rowan, F., Docherty, N.G., Murphy, M., Murphy, B., Calvin Coffey, J., O'Connell, P.R., 2010. Desulfovibrio bacterial species are increased in ulcerative colitis. Dis Colon Rectum 53(11):1530-1536.

Figure legends

Figure 1: AMPKα1 and AMPKα2 deletion in mouse GI tract.
(A) Western blot analysis of AMPKα1, α2, β1, β2, γ1 and γ2 expression in intestinal epithelial cells (IECs) isolated from the duodenum, jejunum, ileum and colon of WT and IEC AMPK KO mice. β-actin was used as loading control. IEC-specific AMPK deletion was obtained by expressing Cre-recombinase driven by the villin promoter. Measurement of (B) body weight, (C) intestine length, (D) colon length, (E) total transit time, and (F) feces humidity in WT and IEC AMPK KO mice. n = 6-8 mice. All data are expressed as means ± SEM. Statistical analysis was performed by using a Student's t test. Black bars, WT mice (WT); White bars, IEC AMPK KO mice (KO).

Figure 2: Absence of IEC AMPK induces an hyperpermeability in distal colon
(A) *In vivo* paracellular intestinal epithelial permeability of WT and IEC AMPK KO mice on regular control diet (CD) determined by measuring the amount of 4 kDa TRITC-dextran in the plasma 4 hours after gavage. n = 3-7 mice per genotype, from three independent experiments. (B) *In vivo* transcellular intestinal epithelial permeability of WT and IEC AMPK KO mice on CD determined by measuring the activity of HRP in the plasma 4 hours after oral gavage. n = 4-6 mice, from three independent experiments. (C) *Ex vivo* paracellular permeability in jejunum, ileum, proximal colon and distal colon WT and IEC AMPK KO mice on CD, evaluated in Ussing chambers by measuring FITC-dextran flux through intestinal segments for 3 hours. n = 7 mice. Statistical analysis was performed by using a Student's t test. (D) *Ex vivo* transcellular permeability in jejunum, ileum, proximal colon and distal colon from WT and IEC AMPK KO mice on CD, evaluated in Ussing chambers by measuring the activity of HRP in the basolateral medium for 3 hours. n = 7 mice. (E) Expression of mRNA for tight junction proteins ZO-1, ZO-2, occludin, claudin 1, claudin 2 and claudin 3 in entire distal colon biopsies from WT and IEC AMPK KO mice. (F) Expression of mRNA for IL-6, TNF-α and IL-1β in entire distal colon biopsies from WT and IEC AMPK KO mice. n = 4-7 mice. All data are expressed as means ± SEM. Statistical analysis was performed by using a Student's t test. *p < 0.05 and ***p < 0.001 indicate a significant increase relative to respective WT intestinal segment. Black bars, WT mice (WT); White bars, IEC AMPK KO mice (KO). G) Schematic summarizing the stress polarity signaling (SPS)-pathway showing impact of AMPK activation/deletion on Ser425 GIV phosphorylation and barrier integrity. (H) Schematic diagram displays the workflow to assess the activation of the SPS pathway in situ in the murine colons, as determined by assessing the abundance of epithelial pS245GIV. (I) Representative images are presented from proximal colon (upper section) and distal colon (lower section) of WT (WT) and IEC AMPK KO (KO) mice without metformin treatment (H_2O) and after administration of 2 mg/ml metformin in drinking water for 5 days (Met). (J) Violin plots display the % area and intensity of pS245 GIV staining as determined by IHC profiler (each dot represents the average of measurements in 4 ROIs, which were assessed in 3-5 images taken from each sample; n = 3 in H_2O group; n = 5 in Met group). Error bars represent SEM. Statistical significance was determined by three-way Anova; **p < 0.01 and ****p < 0.0001.

Figure 3: Deletion of IEC AMPK does not exacerbate permeability and inflammation in colon after a HFD challenge.
(A) Experimental timeline for control diet (CD) or high-fat diet (HFD) challenge for 10 weeks in male WT and IEC AMPK KO mice. (B) *In vivo* paracellular intestinal epithelial permeability of WT and IEC AMPK KO mice on HFD determined by measuring the amount of 4 kDa TRITC-dextran in the plasma 4

hours after gavage. n = 3-7 mice, from three independent experiments. (C) *Ex vivo* paracellular permeability in distal colon of WT and IEC AMPK KO mice on CD or HFD diet. Permeability was evaluated in Ussing chambers by measuring FITC-dextran flux through intestinal segments for 3 hours. n = 7-12 mice. (D) Expression of mRNA for ZO-1 in the intestinal epithelial layer (IEL) fraction isolated from distal colon of WT and IEC AMPK KO mice fed a CD or HFD. n = 7 mice. (E) Expression of mRNA for IL-6, TNF-α, and IL-1β in the lamina propria layer (LPL) fraction isolated from distal colon of WT and IEC AMPK KO mice fed a CD or HFD. n = 7 mice. (F) Circulating IL-6, TNF-α, and IFN-γ levels in WT and IEC AMPK KO mice fed a CD or HFD. n = 5-7 mice. All data are expressed as mean fold change relative to WT. Statistical analysis was performed by two-way ANOVA with Bonferroni post hoc test. *p < 0.05 and **p < 0.01 indicate a significant difference to respective WT intestinal segment and diet challenge. $p < 0.05 and $$$p < 0.001 indicate diet effect within genotype. CD, control diet; HFD, high-fat diet; Black bars, WT mice; White bars, IEC AMPK KO mice.

Figure 4: Deletion of IEC AMPK does not worsen HFD-induced obesity.

(A) Body weight monitoring in WT and IEC AMPK KO mice on control diet (CD) or high-fat diet (HFD) for 10 weeks. n = 5-7 mice. (B) Body weight, body composition examination (expressed as percentage of fat mass and lean mass relative to total body mass), body fat mass and body lean mass measured by nuclear magnetic resonance in WT and IEC AMPK KO mice at the end of CD and HFD challenge. n = 5-7 mice. (C) Daily food intake of WT and IEC AMPK KO mice on CD or HFD. (D) Daily drink intake of WT and IEC AMPK KO mice on CD or HFD. (E) Daily spontaneous locomotor activity of WT and IEC AMPK KO mice. (F) Energy expenditure of WT and IEC AMPK KO mice on CD or HFD during the light and dark phases. (G) O_2 consumption of WT and IEC AMPK KO mice on CD or HFD during the light and dark phases. (H) CO_2 production of WT and IEC AMPK KO mice on CD or HFD during the light and dark phases. (I) Respiratory exchange ratio (VCO_2/VO_2) of WT and IEC AMPK KO mice fed a CD or HFD during the light and dark phases. All calorimetry data are representative of 5 days measurement; n = 6 mice. All data are expressed as means ± SEM. Statistical analysis was performed by two-way ANOVA with Bonferroni post hoc test. °°p < 0.01 and °°°p < 0.001 indicate a diet effect in WT mice. §p < 0.05 and §p < 0.001 indicate a diet effect in IEC AMPK KO mice. $p < 0.05 and $$$p < 0.001 indicate a diet effect within genotype. ##p < 0.01 and ###p < 0.001 indicate a light/dark phase effect within genotype. CD, control diet; HFD, high-fat diet; Black bars, WT mice; White bars, IEC AMPK KO mice.

Figure 5: Deletion of IEC AMPK does not worsen obesity-induced metabolic dysfunctions and does not affect response to metformin.

(A) Blood glucose profile during glucose tolerance test in WT and IEC AMPK KO mice on control diet (CD) or high-fat diet (HFD) . AUC, area under the curve was calculated. n = 5-7 mice. (B) Blood glucose profile during insulin tolerance test in WT and IEC AMPK KO mice on CD or HFD. n = 5-7 mice. (C) Blood glucose profile during metformin tolerance test in WT and IEC AMPK KO mice on CD. Mice were given an oral gavage dose of 250 mg/kg metformin and after 30 minutes challenged with an oral administration of glucose. n = 7-8 mice per genotype. (D) Blood glucose profile during metformin tolerance test in WT and IEC AMPK KO mice on HFD. Mice were given an oral gavage dose of 250 mg/kg metformin and after 30 minutes challenged with an oral administration of glucose. n = 5-7 mice. All data are expressed as means ± SEM. Statistical analysis was performed by two-way repeated measures ANOVA or two-way ANOVA with Bonferroni post hoc test. Black bars, WT mice; white bars, IEC AMPK KO mice. ##p < 0.01 and ###p < 0.001 indicate a diet or metformin effect in WT mice. §p < 0.05, §§p < 0.01 and §§§p < 0.001 indicate a diet or metformin effect in IEC AMPK KO

mice. $p < 0.05, $$p < 0.01 and $$$p < 0.001 indicate a diet or metformin effect within genotype. CD, control diet; HFD, high-fat diet; Black bars, WT mice; White bars, IEC AMPK KO mice.

Figure 6: Inducible deletion of gut AMPK does not exacerbate the development of HFD-induced obesity and metabolic dysfunctions.

(A) Experimental timeline for tamoxifen treatment and control diet (CD) or high-fat diet (HFD) challenge for 16 weeks in male WT and i-IEC AMPK KO mice. (B) Western blot analysis of AMPKα, phospho-AMPKα-Thr172, ACC and phospho-ACC-Ser79 expression in intestinal epithelial cells isolated from ileum of WT and i-IEC AMPK KO mice at the completion of CD or HFD challenge. β-actin was used as loading control. (C) Body weight monitoring in WT and i-IEC AMPK KO mice on CD or HFD for 16 weeks. n = 7-13 mice. (D) Body weight and body composition examination (expressed as percentage of fat mass and lean mass relative to total body mass) in WT and i-IEC AMPK KO mice at the end of CD or HFD challenge. n = 7-13 mice. (E) Blood glucose profile during glucose tolerance test in WT and i-IEC AMPK KO mice on CD or HFD. AUC, area under the curve was calculated. n = 6-11 mice. All data are expressed as means ± SEM. Statistical analysis was performed by two-way repeated measures ANOVA or two-way ANOVA with Bonferroni post hoc test. ##p < 0.01 and ###p < 0.001 indicate a diet effect in WT mice. §§p < 0.01 and §§§p < 0.001 indicate a diet effect in i-IEC AMPK KO mice. $p < 0.05 and $$$p < 0.001 indicate a diet effect within genotype. CD, control diet; HFD, high-fat diet; Black bars, WT mice; Dashed bars, i-IEC AMPK KO mice.

Figure 7: Effect of inducible deletion of IEC AMPK on gut microbiota in mice on CD and HFD.

(A) Principal coordinate analysis (PCoA) based on unweighted UniFrac distance between samples from WT and i-IEC AMPK KO mice on control diet (CD) and high-fat diet (HFD). (B) Shannon index representing α-diversity of microbial communities of WT and i-IEC AMPK KO mice on CD and HFD. The box-plots for each α-diversity metric and the pairwise comparisons between the groups using *t* tests with pooled SD and Bonferroni correction are shown (C) Relative abundance of bacterial orders in WT and i-IEC AMPK KO mice on CD and HFD. (D) Heatmap of bacterial genera abundance in each subgroup. The color scale represents the $\log_{10}$+1 transformed abundance. '_f' or '_g' at the end of taxon name indicate unidentified families or genera, respectively. Linear discriminant analysis (LDA) effect size (LEfSE) score was calculated to evaluate bacterial families or genera overrepresented between WT and i-IEC AMPK KO mice on CD (E) or high-fat (F) diet. n = 7-13 mice. CTL_WT: CD-fed WT mice; CTL_KO: CD-fed i-IEC AMPK KO mice; HFD_WT: HFD-fed WT mice; HFD_KO: HFD-fed i-IEC AMPK KO mice. Black bars, WT mice; Grey bars, i-IEC AMPK KO mice.

Figure 8: Inducible deletion of intestinal AMPK does not worsen obesity-induced permeability and inflammation in colon.

(A) *In vivo* paracellular intestinal epithelial permeability of WT and i-IEC AMPK KO mice on control diet (CD) or high-fat diet (HFD) determined by measuring the amount of 4 kDa TRITC-dextran in the plasma 4 hours after gavage. n = 7-13 mice. (B) *Ex vivo* paracellular permeability in distal colon from WT and i-IEC AMPK KO mice on CD or HFD, evaluated in Ussing chambers by measuring TRITC-dextran flux through intestinal segments for 3 hours. n = 3-6 mice. (C) Expression of mRNA for IL-6, TNF-α, and IL-1β in the distal colon of WT and i-IEC AMPK KO mice on CD or HFD. n = 6-13 mice. (D) Lipocalin-2 (Lcn-2) levels in feces from WT and i-IEC AMPK KO mice on CD or HFD. n= 4-10 mice. (E) Circulating IL-6, TNF-α, and IFN-γ levels in WT and i-IEC AMPK KO mice on CD or HFD. n = 3-6 mice (F) Expression of mRNA for ZO-1 and occludin in distal colon of WT and i-IEC AMPK KO mice on CD or

HFD. n = 6-13 mice. All data are expressed as means ± SEM. Statistical analysis was performed by two-way ANOVA with Bonferroni post hoc test. *p < 0.05, **p < 0.01 and ***p < 0.001 indicate significant increase in dextran flux relative to respective WT intestinal segment and diet challenge. CD, control diet; HFD, high-fat diet; Black bars, WT mice; Dashed bars, i-IEC AMPK KO mice.

Supplementary figure legends

Supplementary figure 1: AMPKα1 and α2 expression in the duodenum crypt-villus axis and along the small intestine in global AMPKα1 and AMPKα2 KO mice.

(A) Western blot analysis of AMPKα1 and AMPKα2 expression in mouse intestinal epithelial samples from duodenum fractionated from villus (F1) to crypt (F4). Expression of proliferating cell nuclear antigen (PCNA), a marker of cell proliferation, was used to monitor the cellular fractionation where the proliferating cells are found in the crypt (F4). β-actin was used as loading control. (B) Quantification of AMPKα1 and AMPKα2 expression along the duodenum crypt-villus axis (from villus [F1] to crypt [F4]) expressed as percent of F1. n = 4. Data are expressed as means ± SEM. Statistical analysis was performed by two-way ANOVA with Bonferroni post hoc test. *p < 0.05 and **p < 0.01 indicate significant change relative to respective F1 fraction. Black bars, AMPKα1; Dashed bars, AMPKα2. (C) Western blot analysis of AMPKα1 and AMPKα2 expression in the duodenum, jejunum and ileum from WT and global AMPKα1 and AMPKα2 KO mice. β-actin was used as loading control. (D) Western blot analysis of AMPKα1 and AMPKα2 expression in the liver and skeletal muscle from WT and IEC AMPK KO mice. β-actin was used as loading control.

Supplementary figure 2: Contractile activity of the GI tract in WT and IEC AMPK KO mice.

(A) Frequency of spontaneous phasic contractions was evaluated for 2 min on jejunum and distal colon longitudinal muscular segments from WT and IEC AMPK KO mice in basal condition and after sequential addition of L-Name (50 µM) and atropine (1 µM). (B) Average tension of jejunum and distal colon longitudinal muscular segments from WT and IEC AMPK KO mice was measured in basal condition and after sequential addition of L-Name (50 µM) and atropine (1 µM). n=8, 2 samples per mice, 4 mice/group. All data are represented as means ± SEM. Statistical analysis was performed by using two-way ANOVA with Bonferroni post hoc test. *p< 0.05 indicates significant change relative to respective WT intestinal segment. Black bars, WT mice; White bars, IEC AMPK KO mice.

Supplementary figure 3 : Analysis of small and large intestine integrity in WT and IEC AMPK KO mice.

(A) Representative hematoxylin and eosin staining in the small and large intestine from WT and IEC AMPK KO mice. Scale bar, 100 µm (B) Ultrastructure of colon from WT and IEC AMPK KO mice observed by transmission electron microscopy. High magnification of intercellular spaces with distinguishable tight junctions are shown (White arrows). Scale bar, 0.5 µm. (C) Expression of mRNA for tight junction proteins ZO-1, ZO-2, occludin, claudin 1, claudin 2 and claudin 3 in entire jejunum, ileum and proximal colon biopsies from WT and IEC AMPK KO mice. n = 4-7 mice. (D) Western blot analysis and quantification of ZO-1 and occludin expression in entire jejunum, ileum, proximal colon and distal colon biopsies of WT and IEC AMPK KO mice. β-actin was used as loading control. (E) Expression of mRNA for IL-6, TNF-α and IL-1β in entire jejunum, ileum and proximal colon biopsies from WT and IEC AMPK KO mice. n = 4-7 mice. All data are expressed as means ± SEM. Statistical

analysis was performed by using a Student's t test. Black bars, WT mice (WT); White bars, IEC AMPK KO mice (KO).

Supplementary figure 4 : Effect of HFD on intestinal epithelial permeability of small and large intestine of WT and IEC AMPK KO mice.

(A) *In vivo* transcellular intestinal epithelial permeability of WT and IEC AMPK KO mice on control diet (CD) and high-fat diet (HFD) determined by measuring the activity of HRP in the plasma 4 hours after oral gavage. n = 6-12 mice, from three independent experiments. (B) *Ex vivo* transcellular permeability in jejunum, ileum, proximal colon and distal colon of WT and IEC AMPK KO mice on CD and HFD, evaluated in Ussing chambers by measuring the activity of HRP in the basolateral medium for 3 hours. n = 7-12 mice. (C) *Ex vivo* paracellular permeability in jejunum, ileum, proximal colon (Prox colon) and distal colon (Dist colon) of WT and IEC AMPK KO mice on CD or HFD diet. Permeabilty was evaluated in Ussing chambers by measuring FITC-dextran flux through intestinal segments for 3 hours. n = 7-12. All data are expressed as means ± SEM. Statistical analysis was performed by two-way ANOVA with Bonferroni post hoc test. CD, control diet; HFD, high-fat diet; Black bars, WT mice; White bars, IEC AMPK KO mice.

Supplementary figure 5: Impact of constitutive intestinal AMPK deletion on obesity-induced metabolic dysfunctions.

(A) Food intake, (B) drink intake and (C) spontaneous locomotor activity of WT and IEC AMPK KO mice on control diet (CD) or high-fat diet (HFD) during the light and dark phases. n = 6 mice. (D) WT and IEC AMPK KO mice were fasted overnight and gavaged with olive oil for an oral fat tolerance test. Plasma triglycerides were measured at the indicated time points. n= 15-17 mice. (E) Plasma lipid parameters in WT and IEC AMPK KO mice on CD or HFD. n= 3-10 mice per genotype. (F) Plasma GLP-1 levels in WT and IEC AMPK KO mice at basal state or 10 minutes after an oral challenge with a glucose/ olive oil mix. n= 7-8 mice per genotype. All data are expressed as means ± SEM. Statistical analysis was performed by two-way repeated measures ANOVA or two-way ANOVA with Bonferroni post hoc test. $p < 0.05, $$p < 0.01 and $$$p < 0.001 indicate a light/dark phase or diet/ bolus challenge effect within genotype. CD, control diet; HFD, high-fat diet; Black bars, WT mice; White bars, IEC AMPK KO mice.

Supplementary figure 6 : Impact of inducible intestinal AMPK deletion on obesity-induced metabolic dysfunctions.

(A) Western blot analysis of AMPKα1 and AMPKα2 expression in IEC from duodenum, jejunum, ileum and colon of WT and i-IEC AMPK KO mice. Inducible IEC-specific AMPK deletion was obtained by expressing a tamoxifen-inducible Cre-recombinase construct driven by the villin promoter and by administering tamoxifen during 5 consecutive days. Mice were investigated 2 weeks after tamoxifen treatment. β-actin was used as loading control. (B) Body fat mass and body lean mass measured by nuclear magnetic resonance in WT and i-IEC AMPK KO mice at the end of CD or HFD challenge. n = 7-13 mice. (C) Number of macrophage, dendritic, neutrophil, monocyte cells in visceral adipose tissue of i-IEC AMPK KO and WT mice fed a normal diet (ND) or high-fat diet (HFD). n= 3-7 per genotype. (D) *Ex vivo* paracellular permeability in jejunum from WT and i-IEC AMPK KO mice on CD or HFD, evaluated in Ussing chambers by measuring TRITC-dextran flux through intestinal segments for 3 hours. n = 3-6 mice per genotype. Data are expressed as means ± SEM. (E) Percentage of macrophage, dendritic, neutrophil, monocyte cells among $CD45^+$cells in the colon of i-IEC AMPK KO

and WT mice on ND or HFD. n= 3-7 mice per genotype. Data are expressed as means ± SEM. Statistical analysis was performed by two-way ANOVA with Bonferroni post hoc test. $$$p < 0.001 indicates diet effect within genotype. CD, control diet; HFD, high-fat diet; Black bars, WT mice; Dashed bars, i-IEC AMPK KO mice.

Author Contributions

Séverine Olivier: Conceptualization; Data curation; Formal analysis; Investigation; Methodology, Writing - original draft. **Camille Pochard**: Conceptualization; Data curation; Formal analysis; Investigation; Methodology, Writing - original draft. **Hanna Diounou**: Investigation. **Vanessa Castillo**: Investigation; Methodology. **Jordane Divoux**: Investigation; Methodology. **Joshua Alcantara**: Investigation; Methodology. **Jocelyne Leclerc**: Investigation; Methodology. **Sandra Guilmeau**: Investigation; Review & editing. **Camille Huet**: Investigation. **Wafa Charifi**: Investigation. **Thibault V. Varin**: Software; Formal analysis; Review & editing. **Noëmie Daniel**: Formal analysis; Investigation; Methodology ; Review & editing. **Marc Foretz**: Funding acquisition; Investigation; Methodology; Resources, Writing - review & editing. **Michel Neunlist**: Funding acquisition; Writing - review & editing. **Benoit L Salomon**: Formal analysis; Funding acquisition; Writing - review & editing. **Pradipta Ghosh**: Formal analysis; Funding acquisition; Writing - review & editing. **André Marette**: Formal analysis; Funding acquisition; Writing - review & editing. **Malvyne Rolli-Derkinderen**: Conceptualization; Data curation; Investigation; Methodology; Project administration; Resources; Supervision; Validation; Writing - original draft and review & editing. **Benoit Viollet**: Conceptualization; Data curation; Formal analysis; Funding acquisition; Investigation; Methodology; Project administration; Resources; Supervision; Validation; Writing - original draft and review & editing.

Acknowledgments

The authors thank the histochemistry and histology, cellular imaging, electron microscopy and cytometry and immunobiology facilities at Institut Cochin for their support. We thank Sophie Thenet (Centre de Recherche des Cordeliers, Paris, France) for the use of Ussing chambers. We thank Grahame Hardie (University of Dundee, Dundee, UK) for generously providing AMPKα1 and AMPKα2 antibodies. The skillful assistance of Julie Jaulin for analysis of contractile activity is gratefully acknowledged.

These studies were supported by grants from Inserm, CNRS, Université de Paris Descartes, Région Ile-de-France, Agence Nationale de la Recherche (ANR-17-CE15-0030 and ANR-19-CE14-0023-01) and Société Francophone du Diabète (allocation de recherche SFD-Industrie 2016 - Pierre Fabre Médicament). S.O. holds a doctoral fellowship from Région Ile-de-France (CORDDIM). P.G., J.A, and V.C were supported by the National Institute of Health (CA238042, AI141630, and CA100768 to P.G).

Figure 1

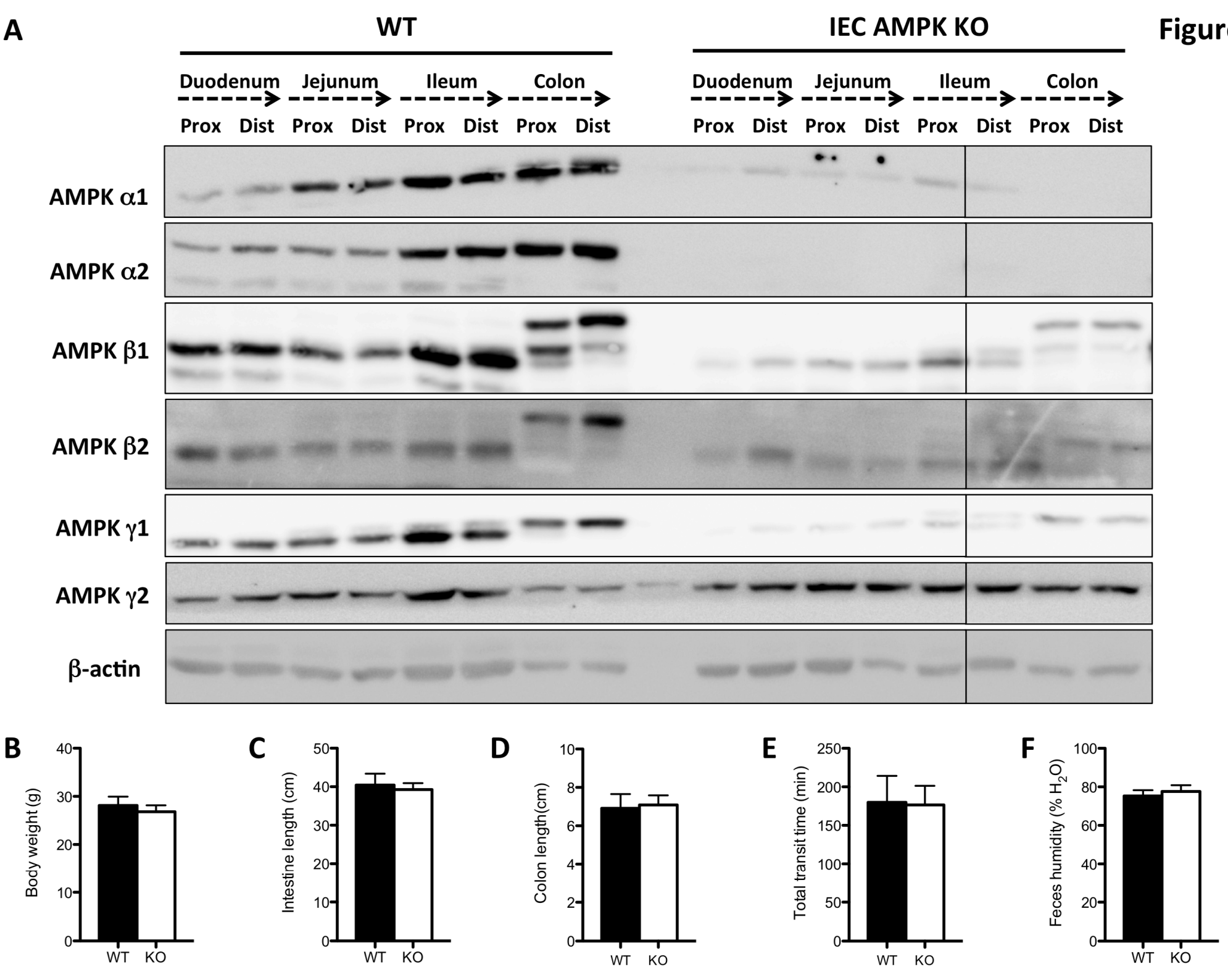

A
WT
IEC AMPK KO
Duodenum
Jejunum
Ileum
Colon
Prox
Dist
AMPK α1
AMPK α2
AMPK β1
AMPK β2
AMPK γ1
AMPK γ2
β-actin
B
Body weight (g)
C
Intestine length (cm)
D
Colon length(cm)
E
Total transit time (min)
F
Feces humidity (% H2O)
WT
KO

Figure 2

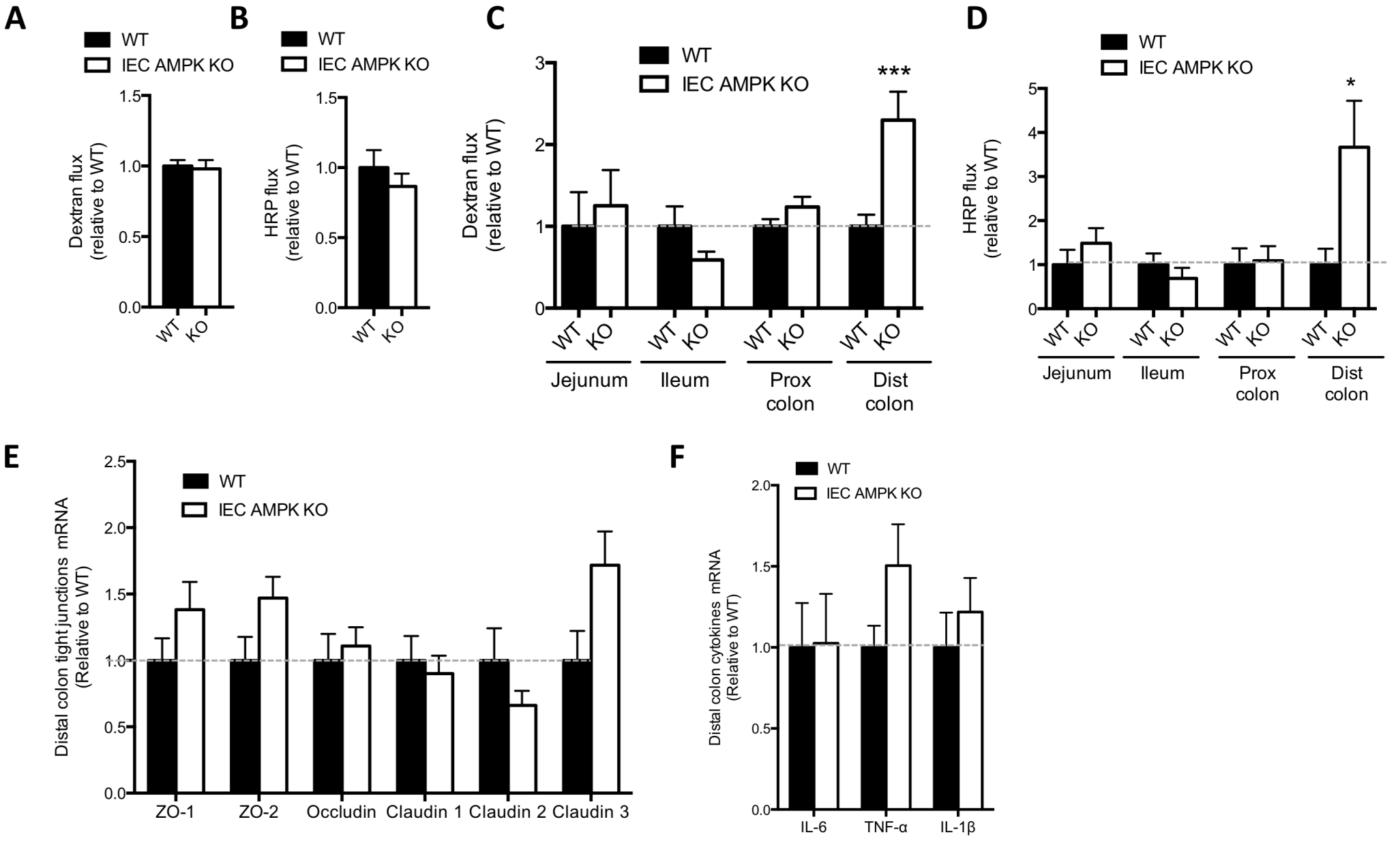

A
B
C
D
WT
IEC AMPK KO
Dextran flux (relative to WT)
HRP flux (relative to WT)
WT
KO
***
*
Jejunum
Ileum
Prox colon
Dist colon
E
F
Distal colon tight junctions mRNA (Relative to WT)
ZO-1
ZO-2
Occludin
Claudin 1
Claudin 2
Claudin 3
Distal colon cytokines mRNA (Relative to WT)
IL-6
TNF-α
IL-1β

Figure 2
(continued)

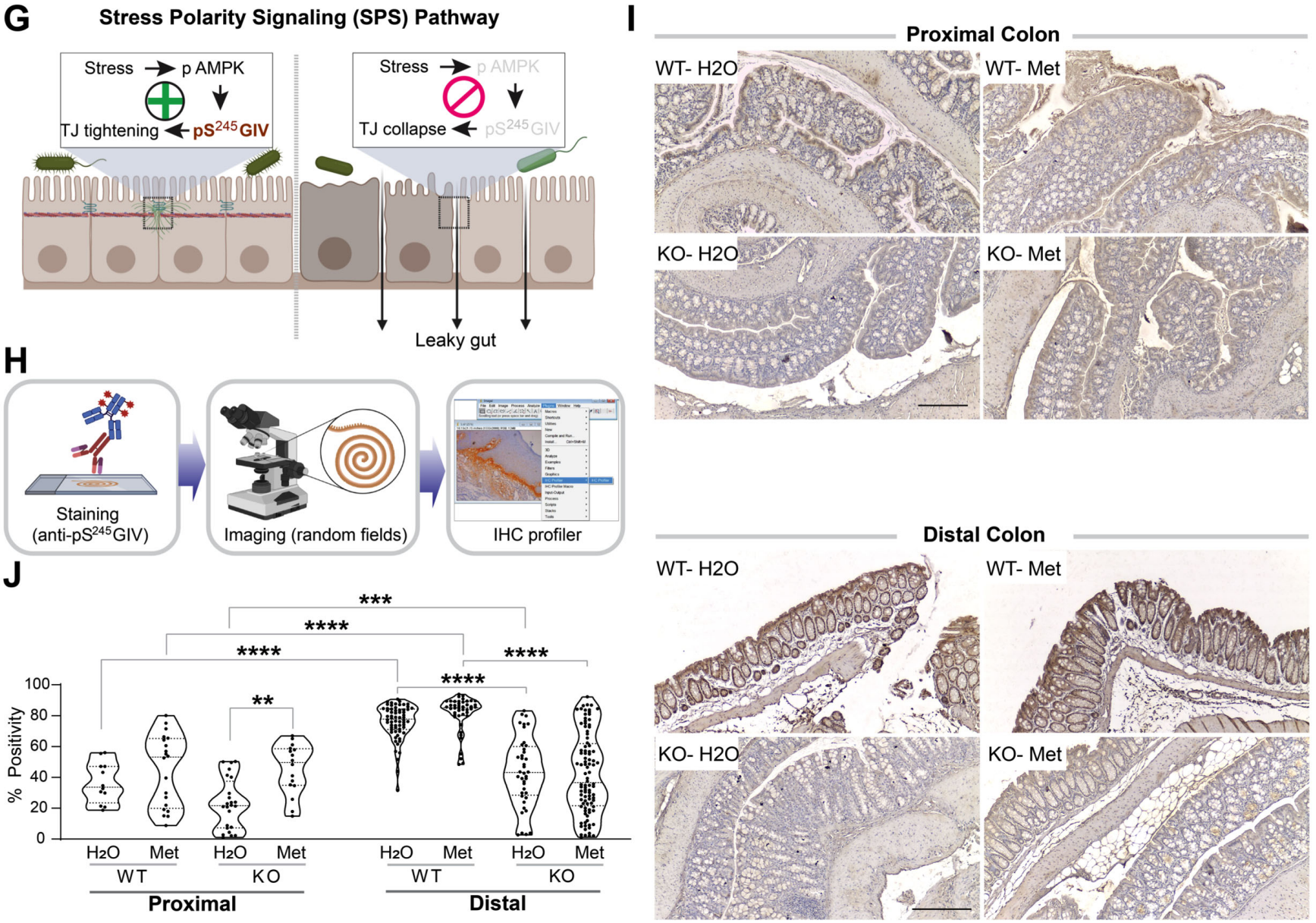


Figure 3

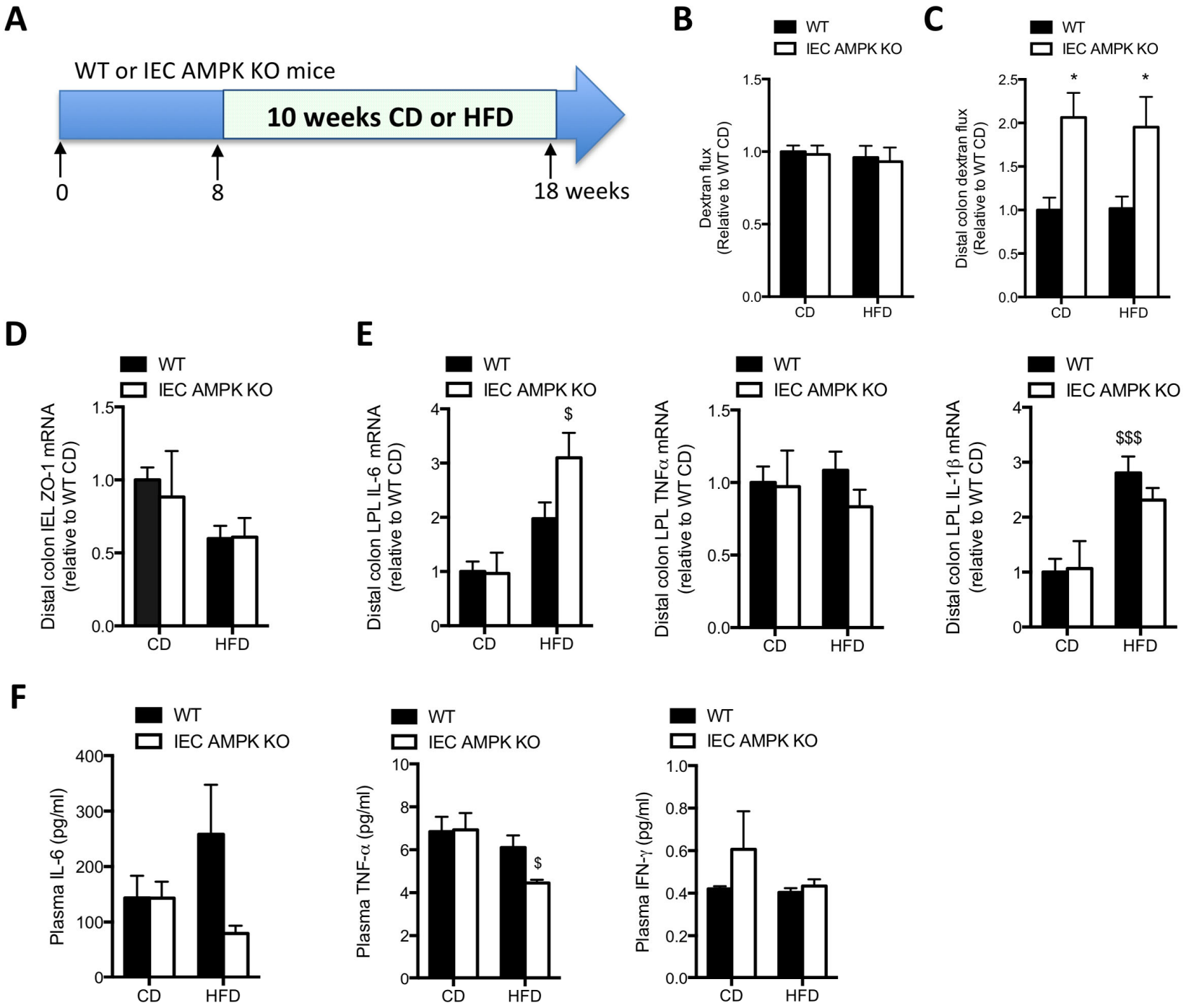

A
WT or IEC AMPK KO mice
10 weeks CD or HFD
0
8
18 weeks
B
WT
IEC AMPK KO
Dextran flux (Relative to WT CD)
CD
HFD
C
Distal colon dextran flux (Relative to WT CD)
*
*
D
Distal colon IEL ZO-1 mRNA (relative to WT CD)
E
Distal colon LPL IL-6 mRNA (relative to WT CD)
$
Distal colon LPL TNFα mRNA (relative to WT CD)
Distal colon LPL IL-1β mRNA (relative to WT CD)
$$$
F
Plasma IL-6 (pg/ml)
Plasma TNF-α (pg/ml)
$
Plasma IFN-γ (pg/ml)

Figure 4

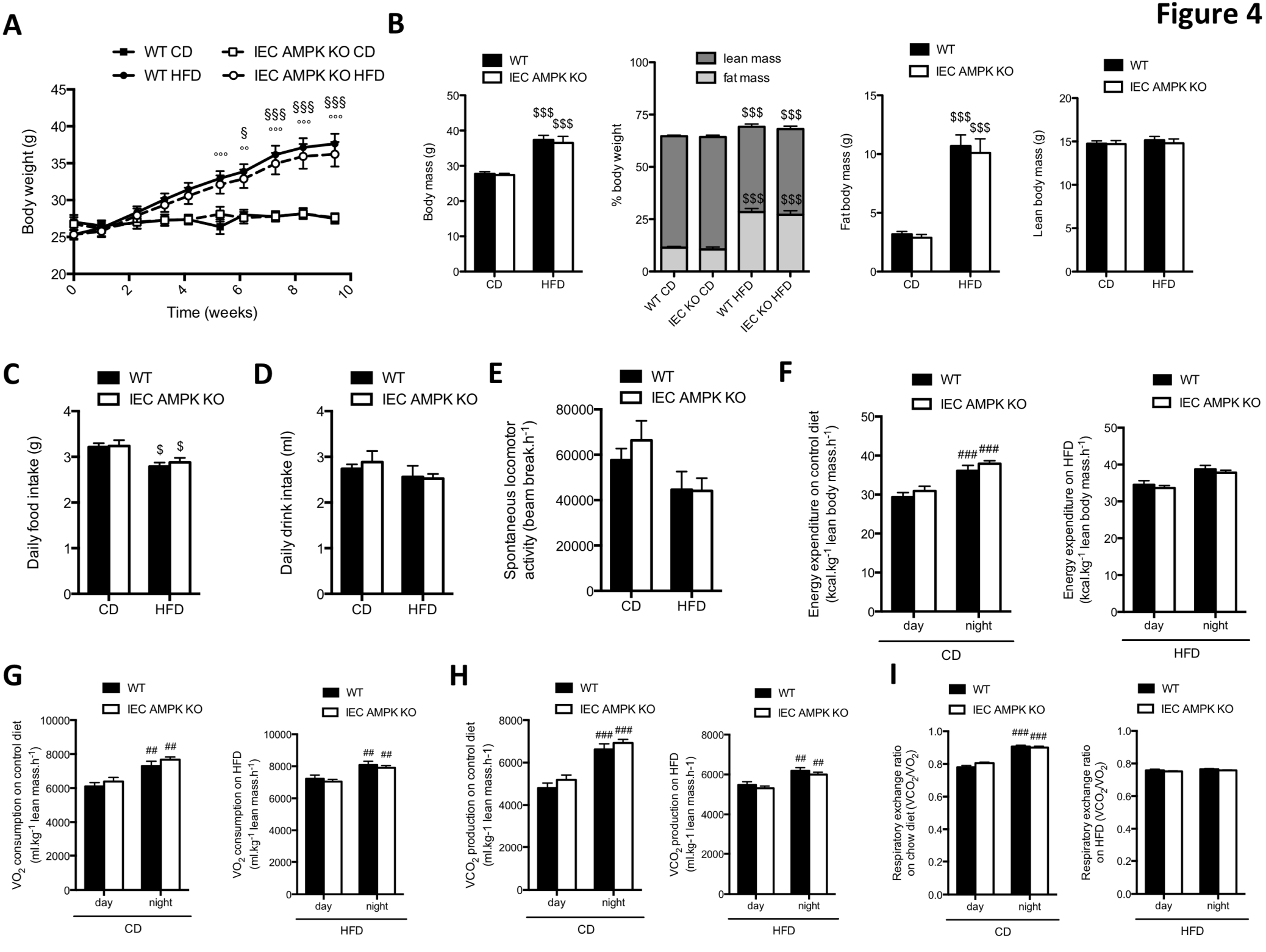

A
WT CD
WT HFD
IEC AMPK KO CD
IEC AMPK KO HFD
Body weight (g)
Time (weeks)
B
WT
IEC AMPK KO
Body mass (g)
CD
HFD
lean mass
fat mass
% body weight
WT CD
IEC KO CD
WT HFD
IEC KO HFD
Fat body mass (g)
Lean body mass (g)
C
Daily food intake (g)
D
Daily drink intake (ml)
E
Spontaneous locomotor activity (beam break.h-1)
F
Energy expenditure on control diet (kcal.kg-1 lean body mass.h-1)
Energy expenditure on HFD (kcal.kg-1 lean body mass.h-1)
day
night
G
VO2 consumption on control diet (ml.kg-1 lean mass.h-1)
VO2 consumption on HFD (ml.kg-1 lean mass.h-1)
H
VCO2 production on control diet (ml.kg-1 lean mass.h-1)
VCO2 production on HFD (ml.kg-1 lean mass.h-1)
I
Respiratory exchange ratio on chow diet (VCO2/VO2)
Respiratory exchange ratio on HFD (VCO2/VO2)

Figure 5

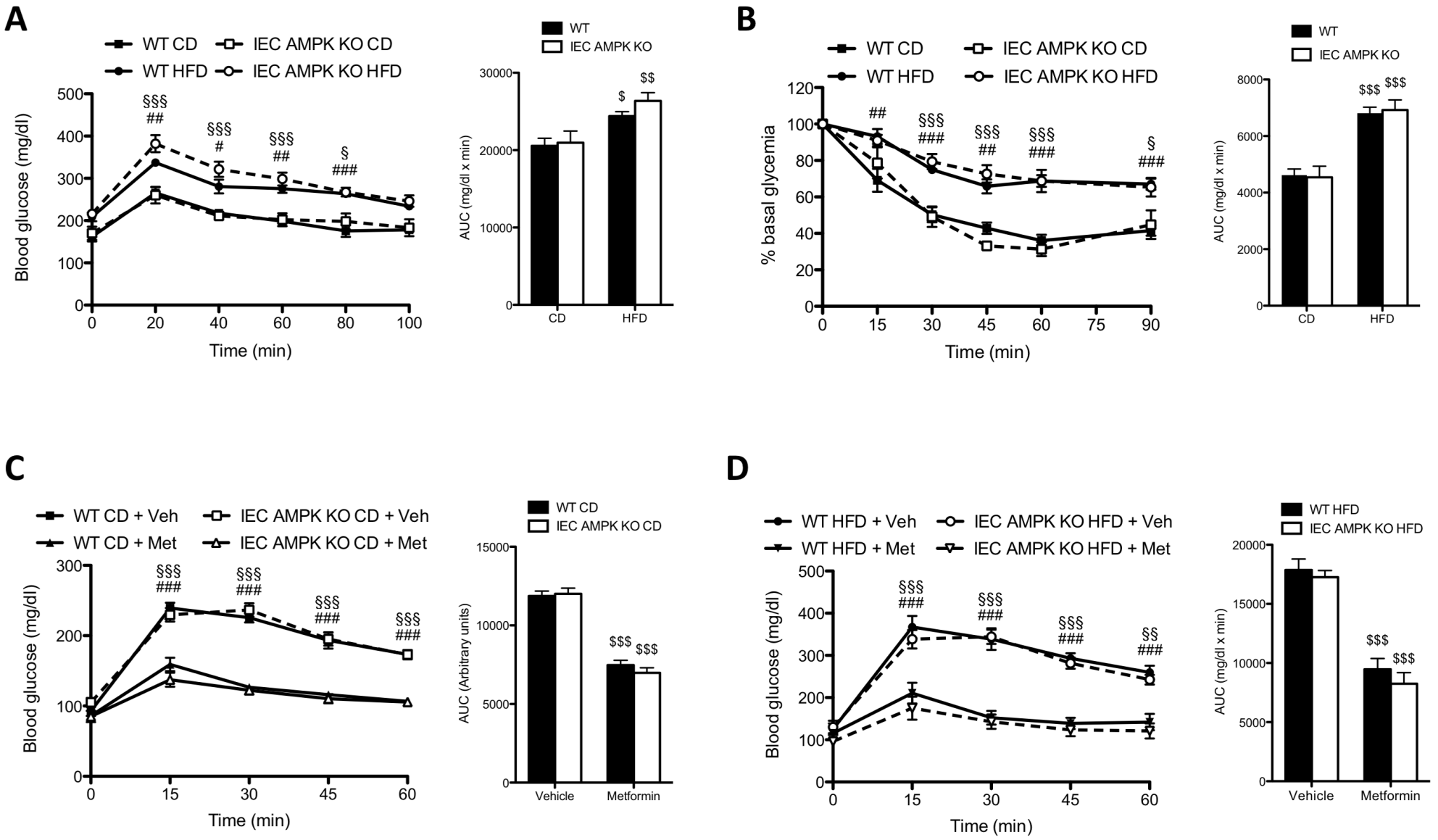
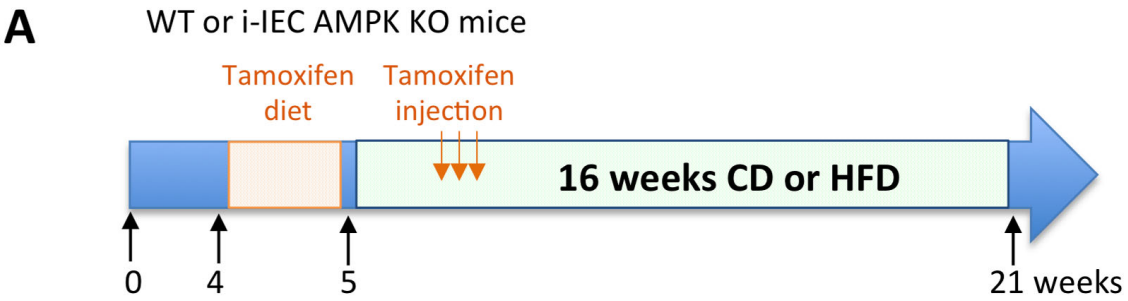
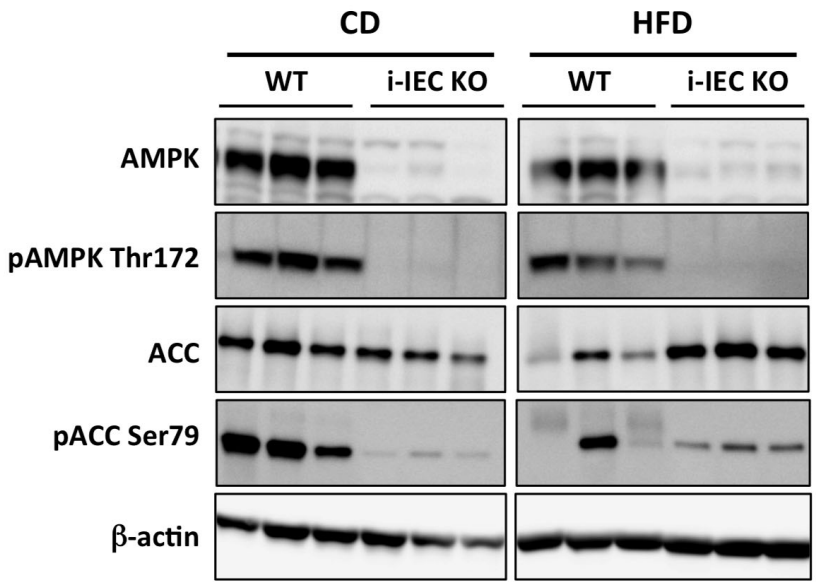
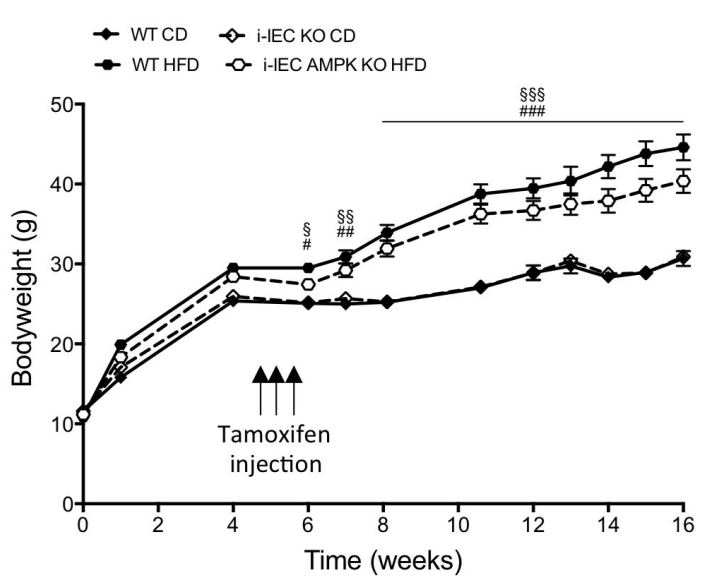

A
WT CD
IEC AMPK KO CD
WT HFD
IEC AMPK KO HFD
Blood glucose (mg/dl)
Time (min)
WT
IEC AMPK KO
AUC (mg/dl x min)
CD
HFD
B
% basal glycemia
C
WT CD + Veh
IEC AMPK KO CD + Veh
WT CD + Met
IEC AMPK KO CD + Met
AUC (Arbitrary units)
Vehicle
Metformin
D
WT HFD + Veh
IEC AMPK KO HFD + Veh
WT HFD + Met
IEC AMPK KO HFD + Met

Figure 6


A
WT or i-IEC AMPK KO mice
Tamoxifen diet
Tamoxifen injection
16 weeks CD or HFD
0
4
5
21 weeks


B
CD
HFD
WT
i-IEC KO
WT
i-IEC KO
AMPK
pAMPK Thr172
ACC
pACC Ser79
β-actin


C
WT CD
i-IEC KO CD
WT HFD
i-IEC AMPK KO HFD
§§§
###
§
#
§§
##
Bodyweight (g)
Tamoxifen injection
Time (weeks)

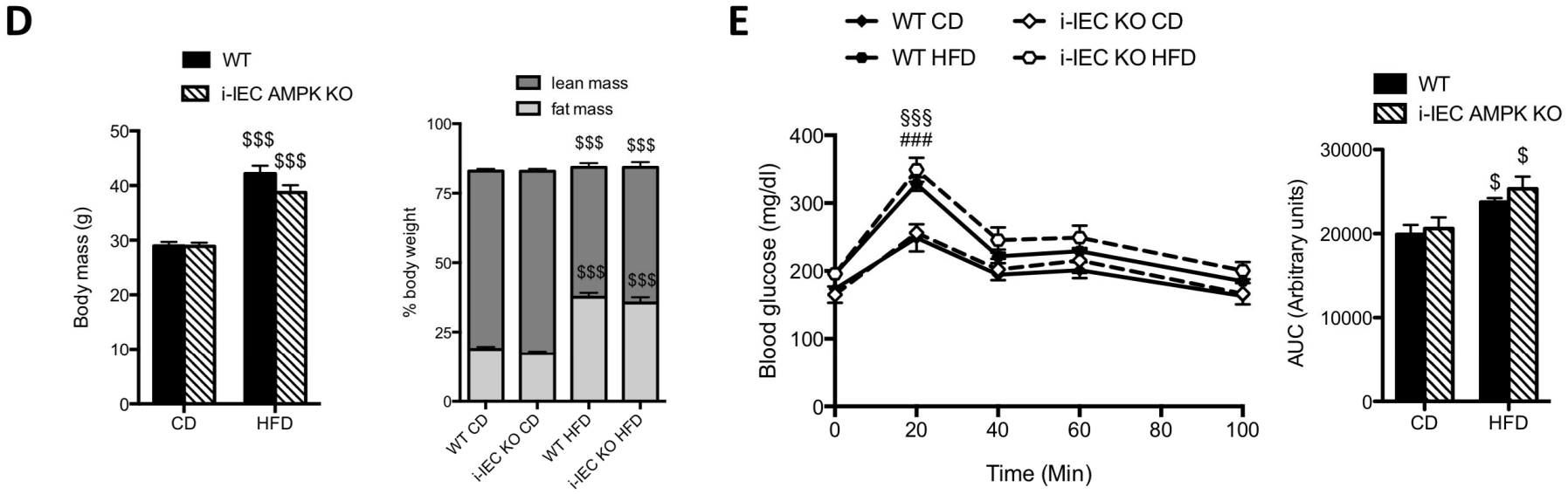

D
WT
i-IEC AMPK KO
Body mass (g)
$$$
$$$
CD
HFD
lean mass
fat mass
% body weight
$$$
$$$
$$$
$$$
WT CD
i-IEC KO CD
WT HFD
i-IEC KO HFD
E
WT CD
i-IEC KO CD
WT HFD
i-IEC KO HFD
§§§
###
Blood glucose (mg/dl)
Time (Min)
WT
i-IEC AMPK KO
AUC (Arbitrary units)
$
$
CD
HFD

Figure 7

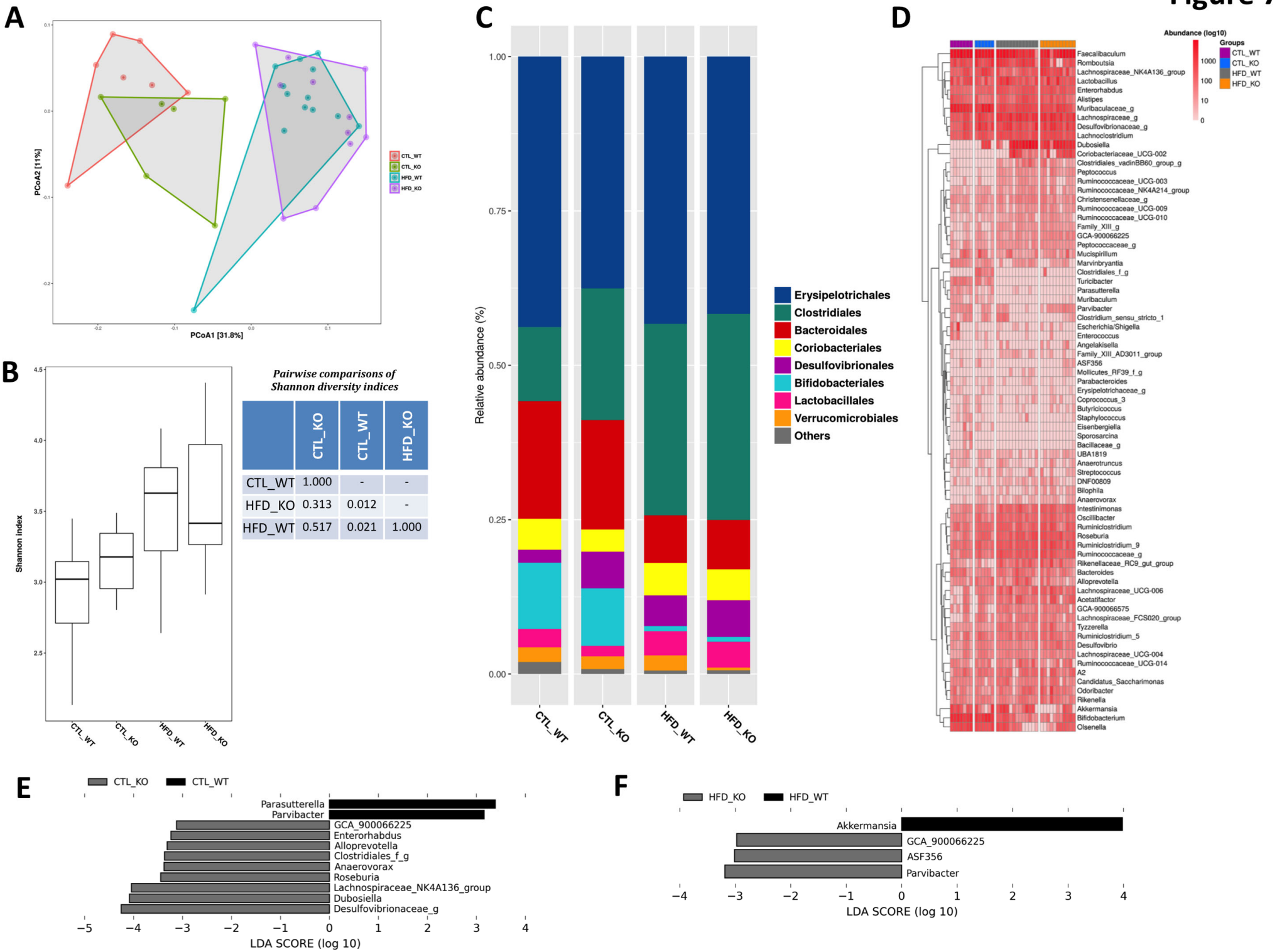
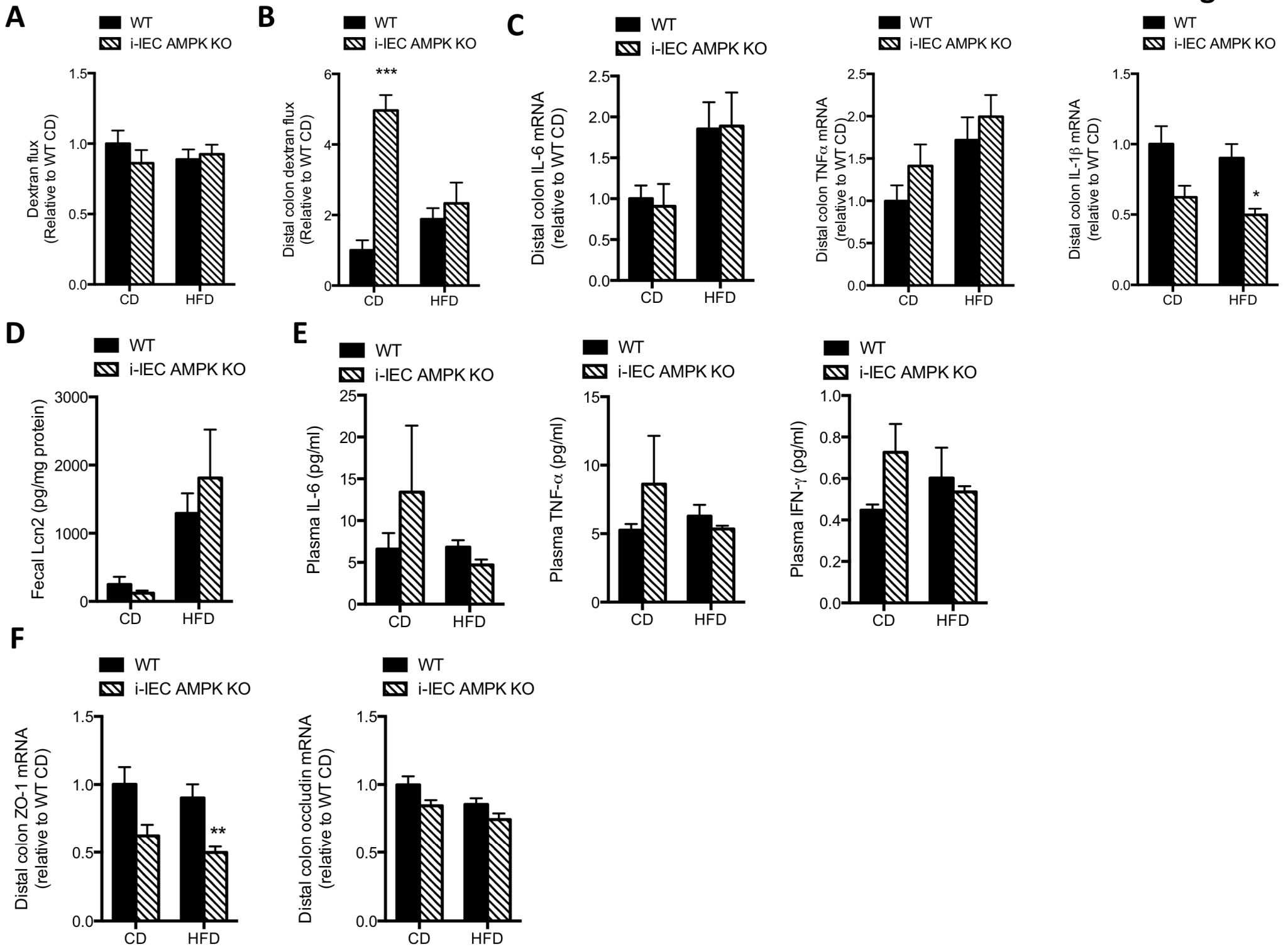

A
PCoA2 [11%]
PCoA1 [31.8%]
CTL_WT
CTL_KO
HFD_WT
HFD_KO
B
Shannon index
CTL_WT
CTL_KO
HFD_WT
HFD_KO
Pairwise comparisons of Shannon diversity indices
CTL_KO CTL_WT HFD_KO
CTL_WT 1.000 - -
HFD_KO 0.313 0.012 -
HFD_WT 0.517 0.021 1.000
C
Relative abundance (%)
Erysipelotrichales
Clostridiales
Bacteroidales
Coriobacteriales
Desulfovibrionales
Bifidobacteriales
Lactobacillales
Verrucomicrobiales
Others
D
Abundance (log10)
Groups
CTL_WT
CTL_KO
HFD_WT
HFD_KO
Faecalibaculum
Romboutsia
Lachnospiraceae_NK4A136_group
Lactobacillus
Enterorhabdus
Alistipes
Muribaculaceae_g
Lachnospiraceae_g
Desulfovibrionaceae_g
Lachnoclostridium
Dubosiella
Coriobacteriaceae_UCG-002
Clostridiales_vadinBB60_group_g
Peptococcus
Ruminococcaceae_UCG-003
Ruminococcaceae_NK4A214_group
Christensenellaceae_g
Ruminococcaceae_UCG-009
Ruminococcaceae_UCG-010
Family_XIII_g
GCA-900066225
Peptococcaceae_g
Mucispirillum
Marvinbryantia
Clostridiales_f_g
Turicibacter
Parasutterella
Muribaculum
Parvibacter
Clostridium_sensu_stricto_1
Escherichia/Shigella
Enterococcus
Angelakisella
Family_XIII_AD3011_group
ASF356
Mollicutes_RF39_f_g
Parabacteroides
Erysipelotrichaceae_g
Coprococcus_3
Butyricicoccus
Staphylococcus
Eisenbergiella
Sporosarcina
Bacillaceae_g
UBA1819
Anaerotruncus
Streptococcus
DNF00809
Bilophila
Anaerovorax
Intestinimonas
Oscillibacter
Ruminiclostridium
Roseburia
Ruminiclostridium_9
Ruminococcaceae_g
Rikenellaceae_RC9_gut_group
Bacteroides
Alloprevotella
Lachnospiraceae_UCG-006
Acetatifactor
GCA-900066575
Lachnospiraceae_FCS020_group
Tyzzerella
Ruminiclostridium_5
Desulfovibrio
Lachnospiraceae_UCG-004
Ruminococcaceae_UCG-014
A2
Candidatus_Saccharimonas
Odoribacter
Rikenella
Akkermansia
Bifidobacterium
Olsenella
E
CTL_KO
CTL_WT
Parasutterella
Parvibacter
GCA_900066225
Enterorhabdus
Alloprevotella
Clostridiales_f_g
Anaerovorax
Roseburia
Lachnospiraceae_NK4A136_group
Dubosiella
Desulfovibrionaceae_g
LDA SCORE (log 10)
F
HFD_KO
HFD_WT
Akkermansia
GCA_900066225
ASF356
Parvibacter
LDA SCORE (log 10)

Figure 8


A
WT
i-IEC AMPK KO
Dextran flux
(Relative to WT CD)
1.5
1.0
0.5
0.0
CD
HFD
B
WT
i-IEC AMPK KO
Distal colon dextran flux
(Relative to WT CD)
***
6
4
2
0
CD
HFD
C
WT
i-IEC AMPK KO
Distal colon IL-6 mRNA
(relative to WT CD)
2.5
2.0
1.5
1.0
0.5
0.0
CD
HFD
WT
i-IEC AMPK KO
Distal colon TNFα mRNA
(relative to WT CD)
2.5
2.0
1.5
1.0
0.5
0.0
CD
HFD
WT
i-IEC AMPK KO
Distal colon IL-1β mRNA
(relative to WT CD)
*
1.5
1.0
0.5
0.0
CD
HFD
D
WT
i-IEC AMPK KO
Fecal Lcn2 (pg/mg protein)
3000
2000
1000
0
CD
HFD
E
WT
i-IEC AMPK KO
Plasma IL-6 (pg/ml)
25
20
15
10
5
0
CD
HFD
WT
i-IEC AMPK KO
Plasma TNF-α (pg/ml)
15
10
5
0
CD
HFD
WT
i-IEC AMPK KO
Plasma IFN-γ (pg/ml)
1.0
0.8
0.6
0.4
0.2
0.0
CD
HFD
F
WT
i-IEC AMPK KO
Distal colon ZO-1 mRNA
(relative to WT CD)
**
1.5
1.0
0.5
0.0
CD
HFD
WT
i-IEC AMPK KO
Distal colon occludin mRNA
(relative to WT CD)
1.5
1.0
0.5
0.0
CD
HFD